OPTICAL NANOSCALE COMMUNICATIONS

Exploring ways towards the excitation and amplification of Surface Plasmon-Polaritons

by

Gonzalo Martínez Soto

May 2015

A master's thesis submitted to the
Faculty of Escola Tècnica Superior
d'Enginyeria de Telecomunicació de Barcelona,
Universitat Politècnica de Catalunya
in conjunction with University at Buffalo,
The State University of New York

Supervisors:
Dr. Josep Miquel Jornet Montaña
Dr. Eduard Alarcón Cot

University at Buffalo
The State University of New York

**UNIVERSITAT POLITÈCNICA
DE CATALUNYA
BARCELONATECH**

Acknowledgements

I would like to dedicate some words to thank all the people without whom this work would not have been possible.

First of all, to my supervisor Dr. Josep Miquel Jornet for giving me the opportunity to work in his research group, where I have learned a lot of new things and discovered the meaning of research. Not only has he been supportive from the very beginning, but also he has guided me through all my work and given me advice whenever I needed it. Thanks to him, I acquired the necessary tools to pursue a research career in the future.

I would also like to thank my parents, my sisters and the rest of my family for their unconditional support, with special mention to my grandmother Ángela, who has helped me pursue my goals.

To my friend Àlex, who has been always there for me, and to all my friends from college (Carles, Dani, David, Francesc, Júlia, Pablo and Pedro), with whom I have shared good and bad moments throughout our studies. Also, to my roommates Brandon and Carl, who have shown me a different side of Western NY and made me feel less far from home.

And last but certainly not least, to my co-supervisor Eduard Alarcón, who gave me a once-in-a-lifetime opportunity to study abroad, for which I will be eternally grateful.

Contents

Contents

List of Figures

List of Tables

Abstract

With the rapidly increasing demand for smaller and faster technology in the world of telecommunications over the past few years, there has come a time for nanotechnology to take over. Nanotechnology will provide with a new set of tools to the engineering community to design and manufacture nanoscale components with unprecedented functionalities. The ability to integrate several of those components into a single structure in just hundreds of nanometers will enable the development of new and advanced nanosystems. In this thesis, we go over the basics of nanoscale communications, the fundamentals of nanonetworks as well as the main state-of-the-art devices proposed to date. As the main focus of this work, two different alternatives to provide a signal source to an optical nanoscale communication system are proposed. First, as the optical term suggests, the basics of the most common light source are covered: the semiconductor laser. We describe its working principles and analyze its capabilities in order to determine its suitability for nanoscale communications. Last, a new concept of light source is proposed, which deals with light-matter interactions in the nanoscale: the plasmon nanolaser.

CHAPTER 1

Introduction

Communication is broadly known as the exchange or transfer of information from one point to another. When the information needs to travel over a considerable distance, a communications system is required. Within a wireless communication system, the exchange of information is accomplished by modulating/encoding that information onto an electromagnetic wave, which acts as a carrier signal. This modulated signal is then transmitted over a channel to its destination, where it is received and the original information is obtained by demodulation.

Over the past few decades, we have seen a major increase in communication technologies. Everyday, there is a crescent demand for smarter and better features, which translates to a better service and reliability. Higher speeds and smarter devices that can integrate more features within less space are some of the main goals to accomplish. Consequently, in order to satisfy those needs we must take a step forward in the research of new techniques and implementations that will grant the development of new and advanced technology.

1

1.1   Optical Communications

Since the 19th century, several techniques have been developed for this process of sending information from one end to another, using carrier waves operating at radio frequencies as well as microwave and millimeter wave frequencies. However, communication may also be achieved using a carrier wave selected from the optical range of frequencies.

The use of visible light for communication has been common for many years. Simple systems such as beacons, smoke signals and heliographs have proved a useful way to send information over the past centuries. However, given that we are living in the 21$^{\text{st}}$ century, we would like to approach this concept of optical communication from the nanoscale point of view: nanophotonics and nanoplasmonics.

1.2   Light as the Carrier Wave

Photons are the elementary particles of light. They have zero rest mass, as well as zero electric charge, thus they are stable. The interesting fact about photons is that they exhibit properties of waves and particles at the same time. Like all elementary particles, however, photons are best explained by quantum mechanics; Nevertheless, if one refers to photons as electromagnetic waves, the classical Maxwell's equations can actually describe light in that sense.

The fact that we choose light to carry information is because not only is much faster than any other technology to date, but allows us to go far beyond from where we are now with other technologies using lower part of the spectrum (i.e., radio frequency). Many applications integrating optics have emerged over the past few years (i.e., telecommunications, biomedical, military), and there are innumerable

yet to be materialized. For example, optical fiber communications are the new way people connect to the Internet from their homes, providing speeds 100x faster than the old ADSL. Or advanced medical equipment that integrates light-based devices that can help to identify and treat diseases, making procedures less invasive for the human body. These are just a glimpse of what we can achieve with light, and there are countless possibilities yet to be discovered.

1.3   Summary of this Work

Addressing the increasing demand for smaller and faster technology, the only way there is to satisfy those needs is making use of nanotechnology, which will provide with a new set of tools to the engineering community to design and manufacture nanoscale components with unprecedented functionalities. The ability to integrate several of those components into a single structure in just hundreds of nanometers (or few micrometers) will enable the development of new and advanced nanosystems [1].

The aim of this thesis is to review and study optical communications in the nanoscale. We will go over the basics of nanoscale communications, the fundamentals of nanonetworks [2] as well as the main state of the art components that take place in our system, stressing the importance of the signal source, which will be the main focus of this work.

1.4   Outline

The remaining of this work is organized as follows. In Chapter 2, we introduce optical nanoscale communications, where we describe the principles in which the

system is based on. Last we review and propose the most suitable components/devices to date that could take place in an optical nanoscale communication system.

In Chapter 3, we propose the first alternative for a light source for an optical communication system, the semiconductor laser. We study its working principle by means of the rate equations, as well as the l-i characteristic. Then we validate the theory presented with a MATLAB simulation of a typical semiconductor laser to analyze its capabilities towards a nanoscale configuration.

In Chapter 4, we propose the second alternative for a light source, the spaser or plasmon nanolaser. Similarly to Chapter 3, we present the fundamental formulation for a plasmonic laser, which is modeled slightly different as we go into the nanometer scale. Then, carry out a simulation of a plasmon nanolaser using COMSOL *Multi-physics*, where we discuss its capabilities and performance against the conventional semiconductor lasers proposed in the previous chapter.

Finally in Chapter 5, we summarize the most important points of this work and we identify the next challenges that need to be tackled in the future.

CHAPTER 2

Optical Nanoscale Communications

In order to get ourselves into optical nanoscale communications, there are some aspects that need to be addressed first. Making use of nanotechnology and thus nanophotonics, there is a need for us to meet the requirements imposed by this technology. Integrating a whole communications system (Figure 2.1) in just several hundreds of nanometers would imply the use of very high radiation frequencies, which would compromise the feasibility of electromagnetic nanonetworks [22]. Therefore, in order for a nanoscale communication system to work, we need to approach the classical electromagnetic theory from a different perspective.

2.1 Fundamentals

The use of nanoscale components and light as our carrier wave give us the key to enable this new technology. Choosing an operating frequency from the range of 400 THz to 700 THz would satisfy one of the principal requirements for nanomachines. But, how can we manage to use light in such nanostructures where the

5
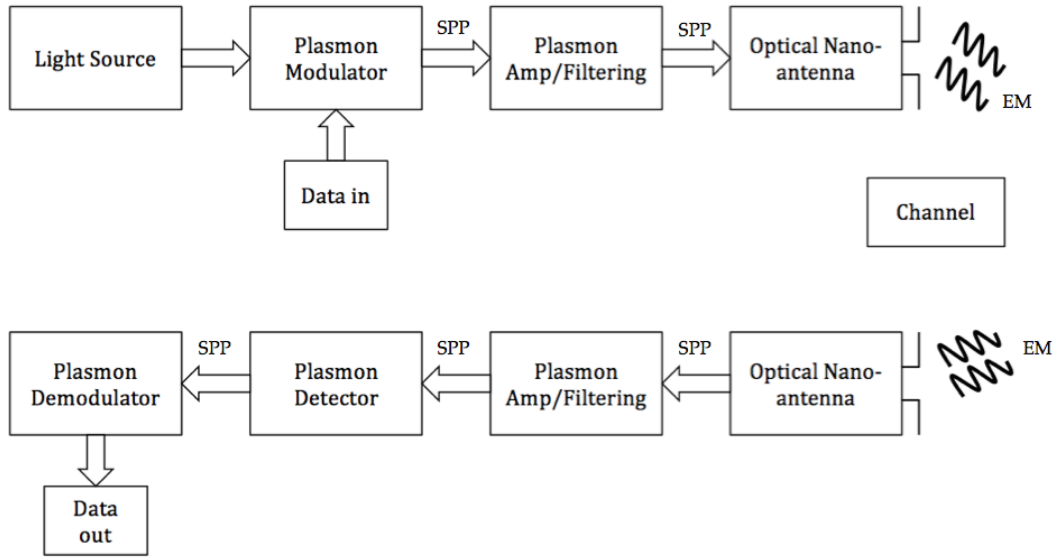
Figure 2.1: Block diagram for an optical nanoscale wireless communication system.

diffraction limit [5] states that it is not possible to localize electromagnetic waves into nanoscale regions much smaller than the operating wavelength?

2.1.1 Diffraction-limited Systems

Diffraction is a phenomenon which occurs when light encounters an obstacle. What happens is when illuminating an object much smaller than the wavelength of the incident light, the latter tends to fade away dramatically. The loss of information arises because light emerging from the object's fine features carries components with high spatial frequency—that is, evanescent waves that exponentially decay. The use of materials with negative permittivity is one of the most feasible ways of bypassing the diffraction limit and achieving localization of electromagnetic fields into nanoscale regions as small as a few nanometers. Noble metals such as gold or silver exhibit negative dielectric permittivity below their plasma frequency [21, 42].

As a result, the use of said materials would support the propagation of surface plasmon-polariton (SPP) waves [27].

2.1.2   Surface Plasmon-Polariton Radiation

SPPs are confined electromagnetic waves coupled to collective electron oscillations at the interface between a metal and a dielectric material. SPP modes existing in metallic nanostructures will lead to the localization of light waves far beyond the diffraction limit for electromagnetic waves in dielectric media, which will only be limited by the atomic structure of matter, dissipation and the spatial dispersion of light.

However, SPPs suffer from high propagation losses, since a significant amount of the SPP field is confined within the metal. For a metal bounded by an ideal dielectric, loss is caused by free-electron scattering in the metal and, at short enough wavelengths (which happens to be our case), by absorption via interband transitions [35]. Although free-electron scattering can be reduced by using advanced fabrication techniques, it cannot be removed completely since the fabrication process has inherent imperfections. Absorption via interband transitions, however, may be avoided by careful selection of the operating wavelength.

Researchers have proposed loss compensation and amplification approaches that add optical gain to the dielectric bounding the metal. In Section 2.2.3 and extensively in Chapters 3 and 4 we will discuss novel techniques that will reduce those SPP high losses and eventually be overcompensated by means of surface plasmon amplification [3].

2.2   System Overview

Having stated the working principles in which our system will be based on, the next step towards getting into optical nanoscale communications is to review the most suitable components reported to date for our system (Figure 2.1).

2.2.1   Light Source

The first and most critical component for our system, is the light source. As we mentioned before, since we are dealing with nanophotonics beyond the diffraction limit [20], we would require some sort of nanoscale photon source capable of enabling those surface plasmon-polariton modes so they could propagate along the system and be radiated by the optical antenna (Section 2.2.5), as well as being able to operate at room temperature. For that reason, a laser-based device would be the best fit, since it would deliver amplified coherent[1] light that could be further converted into SPP radiation. However, as we will see in Chapter 3 and throughout all this work, lasers as we know them do not seem to be the best choice for a nanoscale communication system—which is why in Chapter 4 we propose an exciting new class of light source.

2.2.2   Plasmon Modulation/Demodulation

The implementation and design of plasmonic modulators/demodulators is strongly influenced by the material used in the waveguide where the SPP modes propagate, as well as the thermo-, electro-optical and nonlinearity properties of this material. And since SPP modes are inherently weak and suffer high propagation

---

[1]All atoms radiate in the same fashion.

losses, the realization of plasmonic modulators/demodulators poses a great challenge. However, long-range SPP-based electro- and thermo-optical modulators have been demonstrated in the recent years [25, 29, 32, 38, 43], which carry out a phase modulation by means of electro-optically changing the refractive index of a nonlinear organic material (Figure 2.2a, [29]), and/or by using thermo-optic Mach-Zehnder interferometric modulators (MZIMs)(Figure 2.2b, [32]). Despite that, it still remains a great challenge to downscale these configurations into the nanometer scale as well as to achieve ultra high modulation speeds.
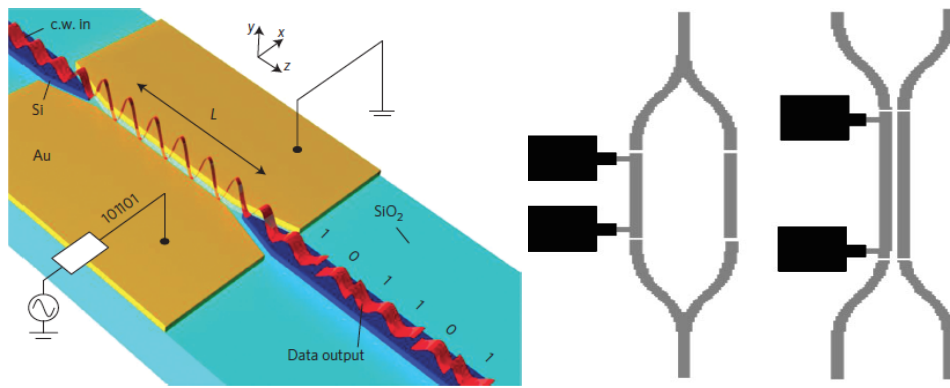
(a) Electro-optic phase modulator from [29].   (b) Mach-Zehnder modulator from [32].

Figure 2.2: High-speed plasmonic phase modulators.

2.2.3 Plasmon Amplification and Filtering

As we mentioned in the previous sections, the realization of SPP-based components constitutes a great challenge because of arduous fabrication processes and inevitable propagation losses that rapidly increase at shorter wavelengths. In spite of that, first designs of nanoscale Fabry-Pérot interferometers based on channel plasmon

waveguiding [36], as well as Mach-Zehnder interferometers and ring resonators [6] have been demonstrated through numerical simulations and found suitable for plasmon routing and filtering. As for plasmon amplification, one way of overcoming SPP losses is to introduce optical gain within the dielectric media bounding the metal. As we will see in Chapter 4, SPP-based lasers [4, 19, 26, 34] constitute a new and revolutionary way to amplify surface plasmons by means of stimulated emission of radiation (SPASERs) [3, 33, 40].

2.2.4 Plasmon Detection

All processes above deal with the generation, amplification and routing of SPP waves. Nevertheless, in the receiver end of our communications system we also require efficient SPP detection so we can further extract the information enclosed in the carrier waves. For that purpose, a few techniques regarding plasmon detection have been proposed in the past few years [16, 18, 30]. The SPP detection configurations were based on SPP coupling to an organic diode, a nanowire field-effect transistor (Figure 2.3b, [18]) and a metal-semiconductor-metal photodetector (Figure 2.3a, [30]), respectively.

2.2.5 Optical Plasmonic Nano-antennas

Optical nano-antennas need to support bandwidths ranging from tens of THz up to several hundreds of THz. The geometry of these antennas makes them suitable for the size requirements of nanotechnology. This type of antennas received attention due to their ability to enhance and focus the emission of single molecules, making them a suitable candidate for sensing applications and small volume spectroscopy [17]. However, as we mentioned in previous sections, metals no longer
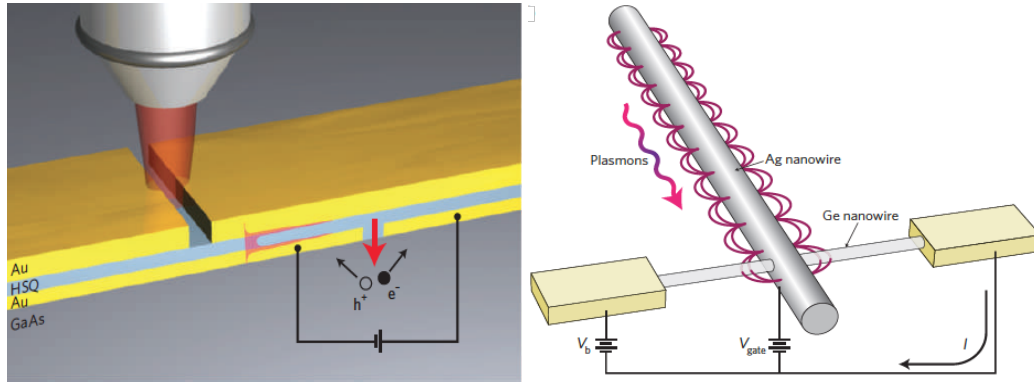
(a) MSM photodetector from [30].   (b) Field-effect transistor detector from [18].

Figure 2.3: Plasmon detection configurations.

behave as perfect electrical conductors (PEC) at such high frequencies, and the material conductivity affects the way in which a current wave propagates in the nano-antenna. In particular, the global oscillations of electrical charge in close proximity to the surface of the antenna results into the excitation of strongly confined EM waves (SPPs). Because of the singularities at optical frequencies, one has to take some considerations in the design of nano-antennas. For example, dipole-like antennas exhibit reflection of the radially polarized surface wave at the end caps (Figure 2.4), which is important in resonance length calculations. Also, previous studies illustrated how the radius of the nanowire can drastically change the propagation properties of the antenna and determine the effective mode index for a cylindrical nano-antenna. Therefore, the choice in the geometry alongside the metal constitutes the main challenge in the design of optical antennas.
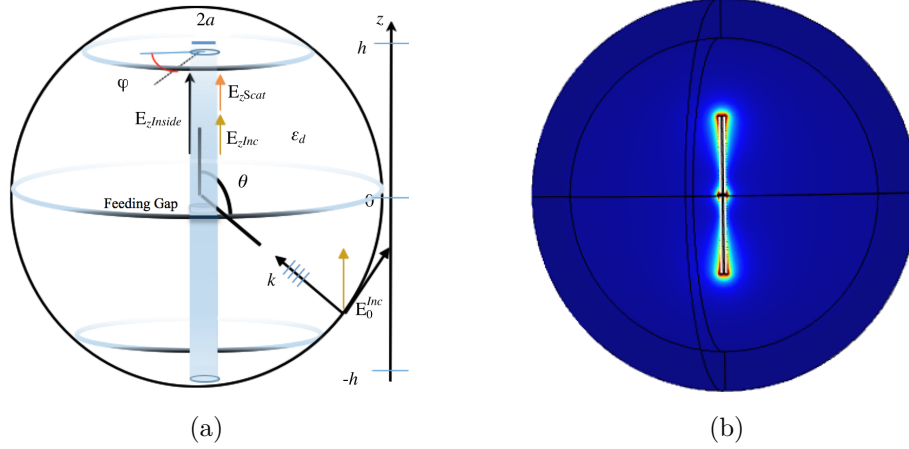
Figure 2.4: Optical antennas. (a) Layout of a dipole-like optical antenna, of length $2h$ and radius a. (b) Shows a 3D simulation result with COMSOL of a dipole-like optical antenna.

2.2.6 Channel Modeling

Channel modeling plays a very important role within a wireless communication system, since it describes how EM waves propagate from one end to another. For nanoscale communications, the intra-body propagation of EM waves at optical frequencies needs to be taken into account. In order to characterize the signal propagation and distortion through multiple layers of different body components, three major channel effects need to be properly studied [24]: i) the absorption, reflection and refraction on the boundaries of different body component layers; ii) the propagation loss due to absorption from each body component layer; iii) scattering due to rough layer boundaries and big cells with comparable size to the optical wavelength (*i.e.*, red and white blood cells).

Intra-body channel modeling poses great challenges due to the complexity of the human body. For example, because of the reflections on multiple layers of body components, an infinite number of paths of the optical waves are formed; or that

the medium permittivity varies significantly in different body components and for different frequency bands. These constitute some of the main problems that need to be solved in the future in order to develop a novel intra-body channel model.

2.3 Outlook

Throughout this chapter we have presented a first approach of our optical communication system, and we have reviewed some of the most recent techniques and devices that manipulate the surface plasmon-polariton waves in terms of generation, amplification, filtering, radiation and so on. As we have mentioned in previous sections, it still remains unknown how to make some of these devices work at deep subwavelength scale as well as at room temperature, since the materials and the SPPs suffer from high losses at optical frequencies. Plasmonics, however, is still at early stages. The realization and integration of all of those plasmonic components into a single nanostructure will represent a groundbreaking milestone for the scientific community.

CHAPTER 3

Semiconductor Lasers

The first approach towards finding a suitable way to generate our main carrier signal is by making use of semiconductor lasers. These are compact-size devices that provide amplified, monochromatic[1], coherent light at the output, which we could use to "illuminate" a plasmon waveguide and excite surface plasmons existing at the interface between the metal and a dielectric layer to further achieve SPP radiation.

In the recent years, subwavelength semiconductor lasers have been proposed [23,31], and have proved to be an effective way to deliver highly coherent light at the output from cavities smaller than the operating wavelength. Moreover, novel techniques allow these devices to work under electrical injection [13–15], which means no optical pumping is required from an external source, and thus they can efficiently work under room temperature. These configurations, however, mostly operate at the telecommunications window[2], which is the most common wavelength range for

---

[1]It contains one specific wavelength/color.
[2]Operating wavelengths around $\lambda = 1.55 \ \mu m$.

these kind of light sources.

In this chapter, we will go over the basics of the semiconductor laser. We will study its dynamic response as well as its behavior to a biased current source. Last, we will analyze the results obtained and determine the feasibility/suitability of this device for our wireless communication system.
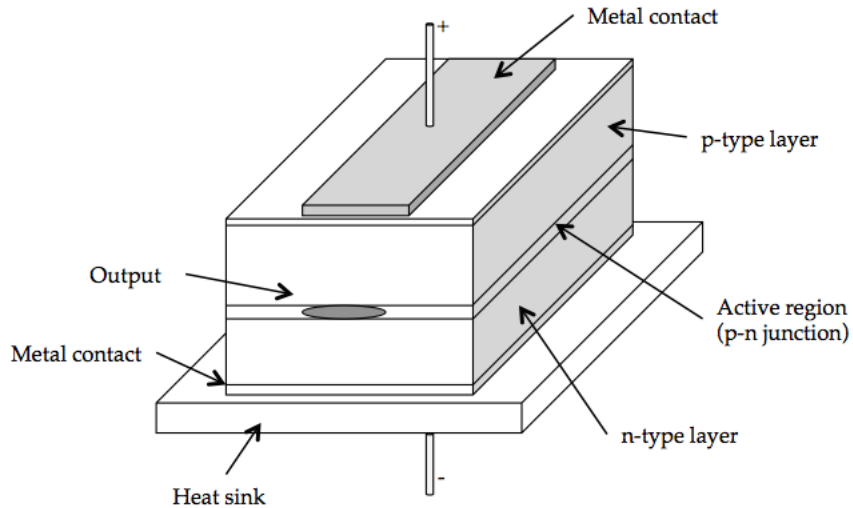
Figure 3.1: Semiconductor laser layout.

3.1   Basics

The term "LASER" is an acronym which stands for **L**ight **A**mplification by **S**timulated **E**mission of **R**adiation. Strictly speaking, a laser is a device which amplifies light. In semiconductor lasers, the optical gain is produced in a semiconductor material. By electrical or optical external pumping, electrons are excited within the conduction band of the semiconductor, resulting in electron-hole pair recombination, which produces spontaneous emission of photons (Figures 3.1

and 3.2). Light amplification is then achieved by means of stimulated emission, in which a photon interacts with the atoms by changing their energy state, stimulating the emission of a second photon, and thus multiplication. In the end, what we have is an optical oscillator in which the photons constantly multiply and form electromagnetic standing waves. At the same time, an external pumping source provides with sufficient energy feedback in order to overcome the cavity losses [39, p. 309-323].
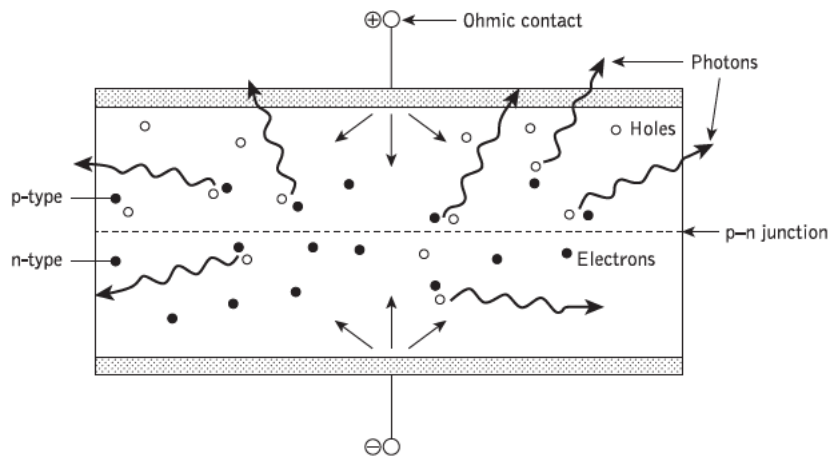
Figure 3.2: Carrier recombination giving spontaneous emission of light [39].

3.2 Rate Equations

In order to describe the laser working principles, in the following sections we will introduce the equations that characterize the dynamic response of a laser. Note that these rate equations can be written in many different ways—depending on the recombination factor of a particular semiconductor, the gain function, and so on. For that matter, we will take a simple version of these equations in order to make the explanations easier to comprehend.

17

3.2.1 Fabry-Pérot Cavity

First, let us assume we have a Fabry-Pérot cavity, which is nothing but an optical cavity with two end facets/mirrors with certain reflectivity indexes R_1 and R_2 respectively (see Figure 3.3).
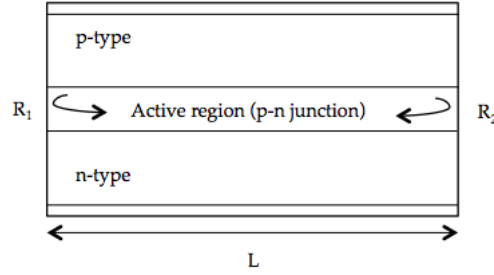
Figure 3.3: Fabry-Pérot cavity.

In order to characterize the Fabry-Pérot cavity, one can find the expression for the change in optical power after one complete roundtrip Υ in the cavity as the following:

$$\Upsilon \equiv R_1 R_2 e^{(\tilde{g}-\alpha_s)2L}, \tag{3.1}$$

where $\tilde{g} = \Gamma g_m$ is the modal gain $[m^{-1}]$, Γ is the confinement factor (see eq. (3.6)) and g_m the material gain, α_s are the intrinsic losses of the waveguide $[m^{-1}]$, where L the cavity length $[m]$ and R_1 and R_2 the facet reflectivities. When g is small such the expression (3.1) is $\ll 1$, any photons injected into the cavity will eventually get lost either because they will leave the cavity through one of the end facets or by being absorbed by the cavity due to its intrinsic losses α_s. But, what if the gain $\tilde{g}$ is made large enough such that (3.1) approaches one? In that case, the number of photons lost from one roundtrip through the cavity would equal the number of

photons generated due to stimulated emission. In other words, the cavity gain per roundtrip would equal the cavity loss per roundtrip. Therefore,

$$R_1 R_2 e^{(\tilde{g}-\alpha_s)2L} = 1 \tag{3.2}$$

represents the lasing condition. When (3.2) is satisfied, large populations of photons can build up inside the cavity starting from spontaneous emission to stimulated emission—therefore achieving laser (light amplification by stimulated emission of radiation). Following expression (3.2), one can find the expression for the gain for which the lasing condition is satisfied. That is,

$$R_1 R_2 e^{(\tilde{g}-\alpha_s)2L} = 1,$$
$$e^{(\tilde{g}-\alpha_s)2L} = \frac{1}{R_1 R_2},$$
$$(\tilde{g} - \alpha_s)2L = \ln\left(\frac{1}{R_1 R_2}\right),$$
$$\tilde{g} - \alpha_s = \frac{1}{2L}\ln\left(\frac{1}{R_1 R_2}\right),$$

thus we obtain

$$\tilde{g} \equiv \tilde{g}_{th} = \alpha_s + \frac{1}{2L}\ln\left(\frac{1}{R_1 R_2}\right), \tag{3.3}$$

where $\tilde{g}_{th}$ is the threshold gain $[m^{-1}]$, which is the minimum gain required to obtain laser. Hence, we now can define the total cavity losses as:

$$\alpha_t = \alpha_s + \frac{1}{2L}\ln\left(\frac{1}{R_1 R_2}\right), \tag{3.4}$$

where α_s are the intrinsic losses of the waveguide $[m^{-1}]$ and

$$\alpha_m = \frac{1}{2L} \ln\left(\frac{1}{R_1 R_2}\right) \tag{3.5}$$

are the losses from the mirrors/facets of the cavity $[m^{-1}]$.

3.2.2 Photon Density Rate Equation

3.2.2.1 Effective Modal Volume

Given the Fabry-Pérot optical cavity (Figure 3.4), the volume of the active region is $V_a = wdL$, which is the product of the width $[m]$, the height $[m]$ and the length $[m]$ of the active region, respectively. Therefore, the area of the active region is $A_a = wh$. In order to define the effective modal volume of the cavity, it is necessary to introduce the confinement factor Γ, which is the ratio between the modal energy in the active region over the total modal energy:

$$\Gamma \equiv \frac{\int_a \varepsilon_o |E|^2 \mathrm{d}r}{\int \varepsilon_o |E|^2 \mathrm{d}r}, \tag{3.6}$$

where $\varepsilon_o = 8.85 \times 10^{-12}\ F/m$ is the vacuum permittivity, and $\vec{E}$ is the electric field $[V/m]$. Then, the effective modal area is defined by $A_{eff} = A_a/\Gamma$ and so the effective modal volume is $V_{eff} = A_{eff} L$.

If we take S' as the total number of photons in the cavity and S as the average photon density in the active region $[m^{-3}]$, one can also find the following relations:

$$\Gamma = \frac{V_a S}{S'}, V_{eff} = \frac{V_a}{\Gamma}, \rightarrow S' = V_{eff} S.$$

For a Fabry-Pérot cavity:

$$V_{eff} = A_{eff}L = \frac{V_a}{\Gamma} = \frac{A_a L}{\Gamma} \rightarrow A_{eff} = \frac{A_a}{\Gamma}.$$
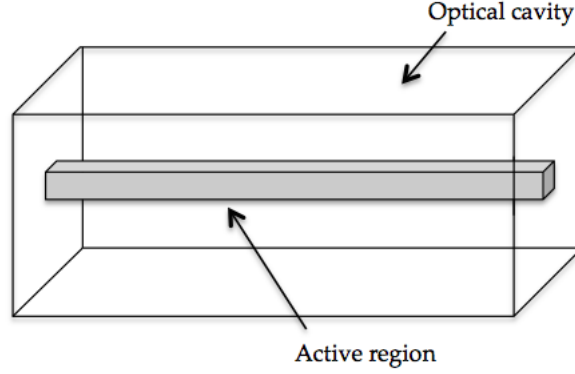
Figure 3.4: 3D view of Fabry-Pérot cavity.

3.2.2.2 Cavity Optical Gain

If we consider an optical cavity with an average photon density S, the rate of stimulated emission in the active region is given by the term $v_g g_m S$, where $v_g = c/n$ is the group velocity $[ms^{-1}]$, $c = 3 \times 10^8 \ ms^{-1}$ is the speed of light in vacuum, n is the refractive index and g_m is the material gain. Now, assuming Fabry-Pérot cavity, the total stimulated emission rate in the active region is $v_g g V_a S$. Then,

$$v_g g V_a S = v_g g S \frac{V_a}{V_{eff}} V_{eff} = \Gamma v_g g_m S'.$$

In terms of average photon density S, the photon multiplication in the cavity due to stimulated emission can be written as:

$$\frac{\partial S}{\partial t} = \Gamma v_g g_m S. \tag{3.7}$$

Note that the term $\Gamma v_g g_m$ expresses the rate at which the number of photons increase inside the cavity due to stimulated emission.

3.2.2.3 Cavity optical loss and photon lifetime

The photon lifetime τ_p expresses the rate at which photons are lost from the cavity, either escaping from the end mirrors or being absorbed by the material. Taking into account this phenomena, we can rewrite (3.7) as:

$$\frac{\partial S}{\partial t} = \left(\Gamma v_g g_m - \frac{1}{\tau_p} \right) S. \tag{3.8}$$

The first term inside the bracket denotes the optical gain, whereas the second term refers to the optical loss. As we stated in (3.2) and (3.3), the condition for lasing is that the optical gain must equal the optical losses. Therefore, the threshold gain g_{th} must satisfy

$$\Gamma v_g g_{th} = \frac{1}{\tau_p}. \tag{3.9}$$

Using the expression obtained in (3.3) and using $\tilde{g} = \Gamma g_m$ and $\tilde{g}_{th} = \Gamma g_{th}$, one can find a new expression for the photon lifetime τ_p as the following:

$$\frac{1}{\tau_p} = v_g(\alpha_s + \alpha_m) = v_g \left(\alpha_s + \frac{1}{2L} \ln \left(\frac{1}{R_1 R_2} \right) \right). \tag{3.10}$$

And since $\alpha_t = \alpha_s + \alpha_m$, the photon lifetime τ_p becomes

$$\tau_p = \frac{1}{v_g \alpha_t}. \tag{3.11}$$

3.2.2.4 Spontaneous Emission Rate

The last term that needs to be considered for the photon density rate equation is the increase in the photon number due to spontaneous emission, which is given by:

$$\beta_{sp} \frac{N}{\tau_s},$$

where β_{sp} is the spontaneous emission factor, N is the carrier density $[m^{-3}]$ and τ_s is the carrier lifetime $[s]$.

Finally, the photon density rate equation can now be written with all its contributions:

$$\frac{\partial S_n}{\partial t} = \left(\Gamma v_g g_{m,n} - \frac{1}{\tau_p} \right) S_n + \beta_{sp} \frac{N}{\tau_s}, \tag{3.12}$$

for $n \in \mathbb{Z}_+$, which represents the optical modes (wavelengths) of operation.

3.2.3 Carrier Density Rate Equation

As we stated in (3.12), the photon density rate equation expresses the increase on the number of photons inside the cavity (due to spontaneous and stimulated emission) and the rate at which the number of photons decrease due to losses in the cavity as well as photons leaving the cavity through the end facets. Similarly to (3.12), the carrier density (N) rate equation can be expressed as:

$$\frac{\partial N}{\partial t} = \eta_i \frac{I}{qV_a} - \frac{N}{\tau_s} - v_g \sum_n g_{m,n} S_n, \tag{3.13}$$

where η_i is the injection efficiency, I $[A]$ is the injection current, $q = 1.602 \times 10^{-19}$ C is the electron charge, V_a $[m^3]$ is the volume of the active region, τ_s is the carrier recombination lifetime $[s]$, v_g is the group velocity $[ms^{-1}]$, $g_{m,n}$ is the material gain $[m^{-1}]$ and S_n the average photon density $[m^{-3}]$ for the n optical mode.

One can easily identify the terms in (3.13) for which the carrier density varies. First term on the right hand of the equation $(\eta_i \frac{I}{qV_a})$ is the rate at which carriers are injected into the cavity. Second term, recombination-generation rate due to spontaneous emission, and the third term is given by all the stimulated emission processes for n wavelengths. Note that the last two terms make the carrier density decrease because of the interaction with photons. Either by spontaneous or stimulated emission, carriers leave their energy states in the active region by producing the emission of photons.

Once we have described both photon and carrier density separately, we now can write down the laser rate equations as follows:

$$\frac{\partial S_n}{\partial t} = \left(\Gamma v_g g_{m,n} - \frac{1}{\tau_p} \right) S_n + \beta_{sp} \frac{N}{\tau_s}, \tag{3.14}$$

$$\frac{\partial N}{\partial t} = \eta_i \frac{I}{qV_a} - \frac{N}{\tau_s} - v_g \sum_n g_{m,n} S_n. \tag{3.15}$$

3.2.4 Material Gain Characterization

Next, in order to characterize the gain, let us assume that the material gain g_m follows the function shown in Figure 3.5 as:

$$g_m = a(N - N_0) - \gamma(\lambda - \lambda_{peak})^2, \tag{3.16}$$

where a is a certain gain coefficient $[m^2]$, N is the carrier density, and N_0 is the carrier density at transparency—that is, assuming the material transparent (no gain). γ is a certain parabolic factor $[m^{-3}]$, λ is the operating wavelength $[m]$, whereas λ_{peak} is the wavelength at which the gain is maximum. In addition, one can extract the following relations from (3.16) and Figure 3.5:

$$g_{peak} = a(N - N_0),$$

$$\Delta\lambda = \sqrt{\frac{2g_{peak}}{\gamma}}.$$
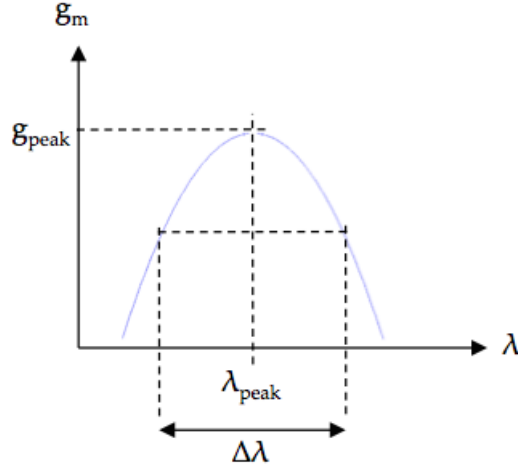
Figure 3.5: Material gain function.

Using the expression for the modal gain $\tilde{g} = \Gamma g_m$, which depends on the material, we obtain:

$$\tilde{g}_n = \Gamma g_{m,n} = \Gamma g_m(\lambda_n) = \Gamma a(N - N_0) - \Gamma\gamma(\lambda_n - \lambda_{peak})^2.$$

Now, assuming we choose the one operating wavelength that maximizes the gain ($\lambda = \lambda_{peak} \rightarrow g = g_{peak}$), the expression for the material gain becomes:

$$g_{m,n} = a(N - N_0),\qquad(3.17)$$

and thus the modal gain becomes

$$\tilde{g}_n = \Gamma a(N - N_0).\qquad(3.18)$$

Once defined the material gain, and assuming we use the wavelength that maximizes the gain for just one optical mode ($n = 1$), we can obtain a new set of rate equations as:

$$\frac{\partial S}{\partial t} = \left(\Gamma a v_g (N - N_0) - \frac{1}{\tau_p}\right) S + \beta_{sp}\frac{N}{\tau_s}$$
$$= \Gamma a v_g (N - N_0) S - \frac{1}{\tau_p} S + \beta_{sp}\frac{N}{\tau_s}.\qquad(3.19)$$
$$\frac{\partial N}{\partial t} = \eta_i \frac{I}{qV_a} - \frac{N}{\tau_s} - v_g a(N - N_0)S$$
$$= \eta_i \frac{I}{qV_a} - \frac{N}{\tau_s} - v_g a(N - N_0)S.\qquad(3.20)$$

And last, substituting $A = \Gamma a v_g$ for a "gain factor", we obtain a new set of coupled laser rate equations:

$$\frac{\partial S}{\partial t} = A(N - N_0)S - \frac{1}{\tau_p} S + \beta_{sp}\frac{N}{\tau_s},\qquad(3.21)$$

$$\frac{\partial N}{\partial t} = \eta_i \frac{I}{qV_a} - \frac{N}{\tau_s} - \frac{A}{\Gamma}(N - N_0)S.\qquad(3.22)$$

3.2.5   Laser Output Efficiency and Power

In order to count the light coming out of the laser, we need to find some expressions related to the output efficiency and output power. Photons may leave the cavity in two different ways; they either get absorbed by the material or they come out of the cavity through the end mirrors. Only the latter constitutes as the laser output. Therefore, we can express the output coupling efficiency as the ratio between the photons leaving the cavity from the mirrors over the total:

$$\eta_0 = \frac{\alpha_m}{\alpha_m + \alpha_s} = \frac{\alpha_m}{\alpha_t}. \tag{3.23}$$

Then, the number of photons leaving the cavity per second is

$$\frac{S'}{\tau_p} = \frac{V_{eff}}{\tau_p} S = \frac{V_a}{\Gamma \tau_p} S,$$

therefore the number of photons leaving from the the end mirrors is

$$\eta_0 \frac{S'}{\tau_p} = \eta_0 \frac{V_{eff}}{\tau_p} S = \eta_0 \frac{V_a}{\Gamma \tau_p} S.$$

Hence, we can express the output power $[W]$ as the number of photons leaving the cavity from the mirrors $\times$ energy of a photon[3]:

$$P_{out} = \eta_0 \frac{V_{eff}}{\tau_p} \hbar \omega S = \eta_0 \frac{V_a}{\Gamma \tau_p} \hbar \omega S. \tag{3.24}$$

---

[3] $E_p = \hbar \omega$ $[eV]$, where $\hbar = \frac{h}{2\pi}$ is the normalized Planck's constant ($h = 6.626 \times 10^{-34}$ $m^2 kg s^{-1}$), and $\omega = 2\pi f$ is the lasing frequency $[rad/s]$.

3.3   Light-Output vs. Current Characteristic

In the previous sections we have described the dynamic response of a semiconductor laser by means of the rate equations. In this section, on the other hand, we want to study the laser response to a biased current source. The nonlinear equations can easily be solved numerically on a computer. However, more insight is obtained solving analytically these equations for different regimes of operation. From now on, we will need to solve Equations (3.21) and (3.22) in steady state for different values of current. Steady state implies $\frac{\partial S}{\partial t} = \frac{\partial N}{\partial t} = 0$, thus:

$$0 = A(N - N_0)S - \frac{S}{\tau_p} + \beta_{sp}\frac{N}{\tau_s}, \tag{3.25}$$

$$0 = \eta_i\frac{I}{qV_a} - \frac{N}{\tau_s} - \frac{A}{\Gamma}(N - N_0)S. \tag{3.26}$$

Rearranging the terms in the equations and taking back the expressions $A = \Gamma a v_g$ and $g_m = a(N - N_0)$ we obtain

$$S = \frac{\beta_{sp}N}{\tau_s\left(\frac{1}{\tau_p} - \Gamma v_g g_m\right)}, \tag{3.27}$$

$$\frac{\eta_i I}{qV_a} = \frac{N}{\tau_s} + v_g g_m S. \tag{3.28}$$

3.3.1   Region I—Laser way below Threshold $(N \ll N_0)$

Let us suppose the current is switched on and is small enough such that $(N \ll N_0)$ and thus the gain is "negative". Any photons emitted spontaneously into the cavity will eventually experience loss, either from the cavity itself (α_s) or from the end mirrors (α_m). Therefore, photons will not last for long inside the cavity so

the average photon density will be practically inexistent (Figure 3.6b, region I).
Hence, one can ignore the stimulated emission term in (3.28) and determine the
carrier density from:

$$\frac{\eta_i I}{q V_a} = \frac{N}{\tau_s}.$$

(3.29)

Once the carrier density has been determined in (3.29), the photon density can be
obtained using (3.27) above (see Appendix A).

3.3.2   Region II—Laser below Threshold $(N_0 < N \ll N_{th})$

As the current increases, the carrier density will also increase as dictated by (3.29)
and at some point, the carrier density will exceed the transparency (Figure 3.6a,
region II) and thus the gain will become positive. Now, photons emitted from
spontaneous emission will eventually be multiplied via stimulated emission. How-
ever, since $N \ll N_{th}$ [4] and so $\tilde{g} \ll \tilde{g}_{th}$, the photon multiplication will not be large
enough to overcome the photon loss in the cavity, therefore the photon density
will still remain considerably small (Figure 3.6b, region II). Once again, one can
ignore the stimulated emission term in (3.28) and determine the carrier density
from (3.29). Once the carrier density has been determined, the photon density
can be obtained using (3.27) above (see Appendix A).

3.3.3   Region III—Laser near Threshold $(N \leq N_{th})$

As the current keeps increasing, it will eventually reach a certain value for which the
carrier density will equal the threshold carrier density N_{th}. The current for which
that happens is called the threshold current, and it is given by (3.29) and (A.8)

---

[4]N_{th} is the threshold carrier density (see Appendix A, Equation (A.8))

for $N = N_{th}$:

$$I_{th} \equiv I(N = N_{th}) = \frac{qV_a}{\eta_i \tau_s} N_{th} = \frac{qV_a}{\eta_i \tau_s}\left(N_0 + \frac{\alpha_t}{\Gamma a}\right).$$ (3.30)

When the carrier density N equals the threshold carrier density N_{th}, the gain $\tilde{g}$ will eventually reach the gain threshold $\tilde{g}_{th}$, and therefore the photon density S (as predicted by (3.27)) will tend to infinity because the denominator would become zero. As a matter of fact, if the carrier density happened to exceed the threshold carrier density and thus the gain exceeded the threshold, the photon density would become negative—which makes no physical sense. As the gain $\tilde{g}$ approaches the threshold $\tilde{g}_{th}$, we can see that in (3.27), the optical gain $\Gamma v_v g_m$ approaches the optical loss $1/\tau_p$ and thus the steady state photon density increases significantly because the denominator tends to zero. When the photon density becomes very

(a) Carrier density N.
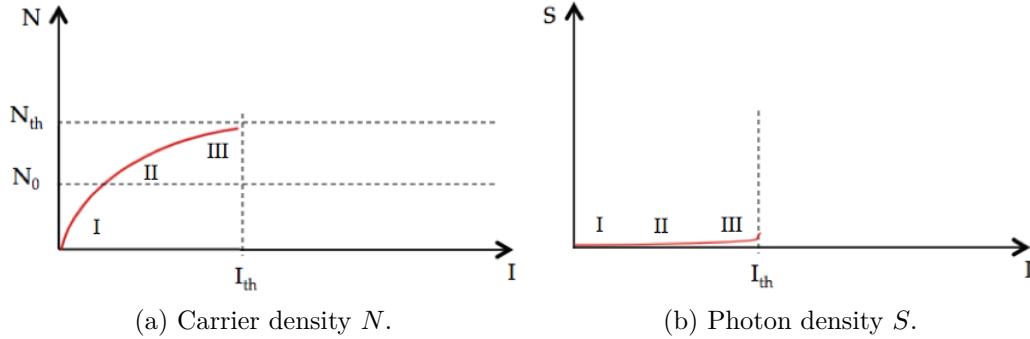
(b) Photon density S.

Figure 3.6: Carrier and photon density vs. current for regions I-III.

large, Equation (3.29) is no longer valid since the carrier recombination term due to stimulated emission cannot be ignored anymore. Hence, we would need to use (3.28) to determine the carrier density in steady state. In Equations (3.27) and (3.28) we can observe that as the photon density increases, the stimulated emission rate $\Gamma v_g g_m S$ also increases and keeps the carrier density (and therefore

the gain) from increasing as much as when the stimulated emission term was ignored. Indeed, when the optical gain $\Gamma v_v g_m$ is close to the optical loss $1/\tau_p$, the increased stimulated emission rate never allows the carrier density to ever exceed the threshold carrier density, and therefore the gain never exceeds the threshold gain. This gain saturation is needed to stabilize the photon density within the cavity, because if the optical gain was to exceed the threshold gain, means that the steady state photon density would have approached an asymptote, hence there would be no steady state—which is why (3.27) predicts a negative photon density for $\Gamma v_g g_m > 1/\tau_p$.

3.3.4 Region IV—Laser above Threshold $(N \approx N_{th})$

As the current increases beyond the threshold current I_{th}, the photon density becomes so large such that the increasing recombination due to stimulated emission prevents the carrier density from increasing above threshold N_{th}. Now, to calculate the photon density for $I > I_{th}$, rearranging (3.28) and (3.30) we have:

$$\frac{\eta_i I}{qV_a} = \frac{N}{\tau_s} + v_g g_m S \qquad (3.31)$$

$$\frac{\eta_i I_{th}}{qV_a} = \frac{N_{th}}{\tau_s} \qquad (3.32)$$

Subtracting (3.32) from (3.31) yields

$$\frac{\eta_i (I - I_{th})}{qV_a} = \frac{N - N_{th}}{\tau_s} + v_g g_m S. \qquad (3.33)$$

Since $I > I_{th}$, assuming $N \approx N_{th}$ makes the first term on the right side of the equation equal to zero, and $\tilde{g} \approx \tilde{g}_{th}$ implies that $\Gamma v_g g_m = 1/\tau_p$.

Therefore, (3.33) becomes

$$S = \Gamma \frac{\eta_i \tau_p}{q V_a} (I - I_{th}). \tag{3.34}$$

Equation (3.34) shows that the photon density increases linearly with the current beyond threshold (Figure 3.7b, region IV). Above threshold, the carrier density and optical gain have reached saturation, which means that the corresponding increase in the stimulated emission rate as the current increases is enough in order to maintain the carrier density close at its threshold value (Figure 3.7a, region IV). As we can see in Figure 3.7b, the photon density clearly shows two different behaviors. From regions I-III, S increases for the most part due to spontaneous emission (since we ignored the stimulated emission term in (3.28)). Then, as the current increases beyond threshold I_{th}, S increases linearly with the current and the contribution is mainly made by means of stimulated emission. The latter region is called *lasing*.

(a) Carrier density N (b) Photon density S
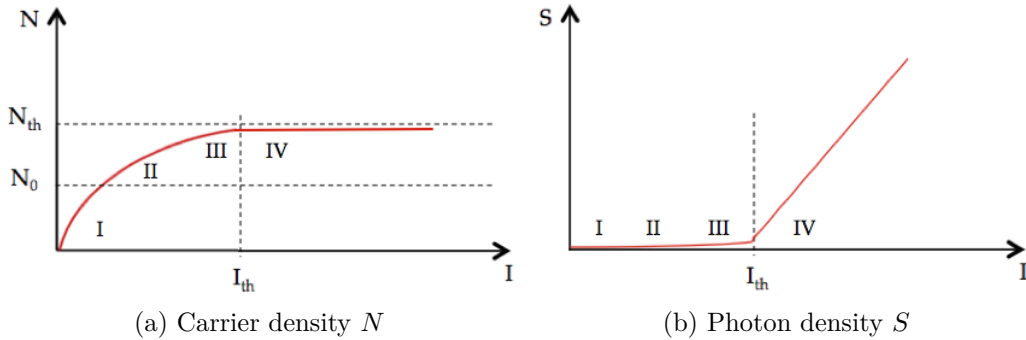
Figure 3.7: Carrier and photon density vs. current for $I > I_{th}$.

3.3.5   Laser Output Power above Threshold $(I > I_{th})$

As we stated in Section 3.2.5, the light coming out of the laser from the end mirrors constitutes the output power:

$$P_{out} = \eta_0 \frac{V_a}{\Gamma \tau_p} \hbar \omega S.$$

And since for $I > I_{th}$, the photon density S is given by

$$S = \Gamma \frac{\eta_i \tau_p}{q V_a}(I - I_{th}),$$

the total output power in terms of the current (I, I_{th}) is

$$P_o = \eta_o \eta_i \frac{\hbar \omega}{q}(I - I_{th}), \tag{3.35}$$

which shows that the output power also increases linearly with the injected current beyond threshold.

3.4   Semiconductor Laser Simulation with MATLAB

In order to validate the results obtained in the previous sections, we carried out a simulation of a basic semiconductor laser using the software MATLAB. For that reason, we chose the typical values in terms of dimensions and operating wavelength so we would be able to illustrate the theory we presented. In Appendix B.1, one can find the basic parameters used for an InGaAs semiconductor laser, and in Appendix B.2 one can find the script in order to run the simulations.

We performed a simulation for both dynamic response of the laser (rate equations) and the output power response to a biased current source. In Figure 3.8 we can

observe the response of the carrier and photon density within the cavity. In the upper graph, we can see how carriers (electrons) start building up inside the cavity until they reach the threshold density N_{th} and then remain at a stable value for the photon density to start increasing. As we mentioned in Section 3.3.3, we can observe in the lower graph how rapidly the photon density varies due to spontaneous emission and losses in the cavity. As the carrier density N stabilizes,
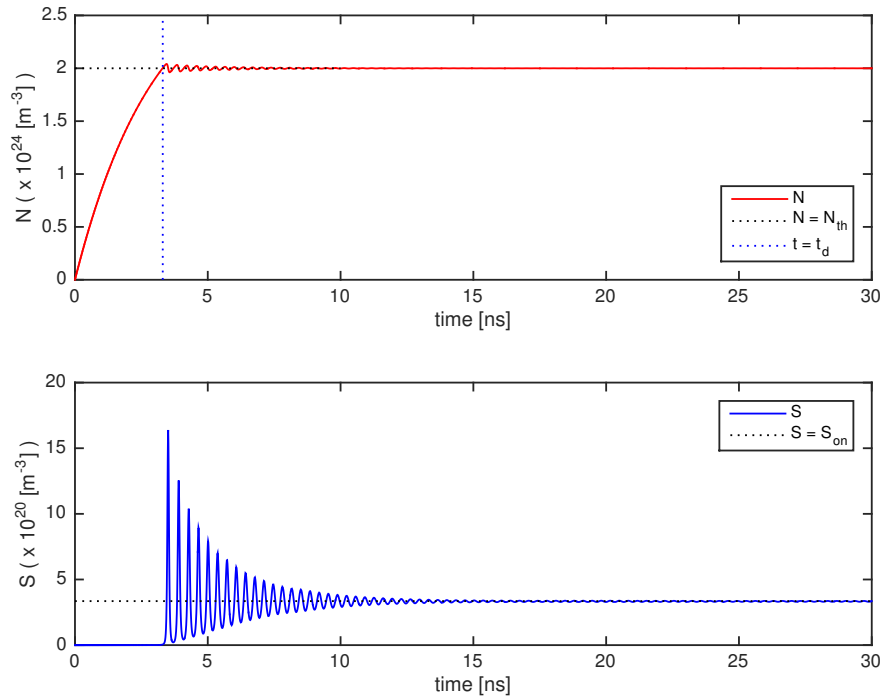
Figure 3.8: Upper graph shows the dynamic response of the carrier density N inside the cavity. Lower graph shows the response of the photon density S inside the active region.

the photon density S begins to settle when stimulated emission kicks in, since the gain increases and tries to compensate the losses. After a small period of time, the

gain overcomes the losses and so the photon density reaches its stable value mainly due to stimulated emission. In the insight on the upper graph in Figure 3.8, we defined a parameter t_d called the switch-on delay, which is the amount of time the laser needs to switch on and start emitting light at the output. As for the photon density graph, we defined the parameter S_{on} which is the photon density level when in lasing mode (stimulated emission). Figure 3.9 shows the power at the
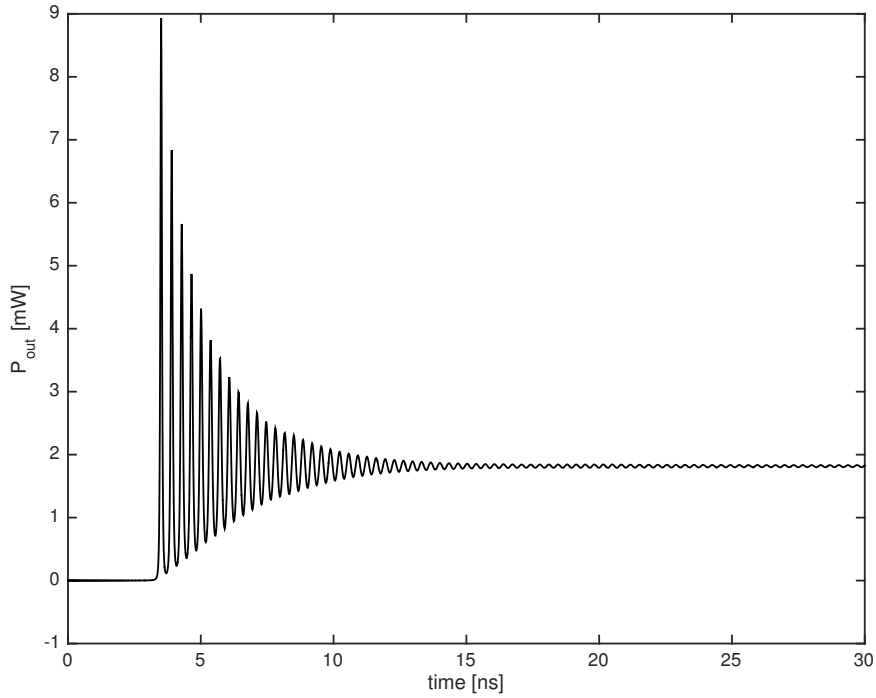
Figure 3.9: Response of the laser output P_{out}.

output P_{out} along time. Similarly to the photon density S in Figure 3.8, the output shows fluctuating values at the beginning mainly because it depends entirely on the photon density. We can see that at first, the power varies rapidly because the gain is still not large enough to overcome the cavity losses. Once the gain reaches

threshold, lasing begins and the laser shows a fairly stable output.

Next, we also wanted to represent what is the laser response to a biased current source. For that matter, in Figure 3.10 we can observe the light output (P_{out}) vs. the current. As we explained in Section 3.3, we can perfectly indentify all the regions in which the laser operates. At first, when the current is switched on, we
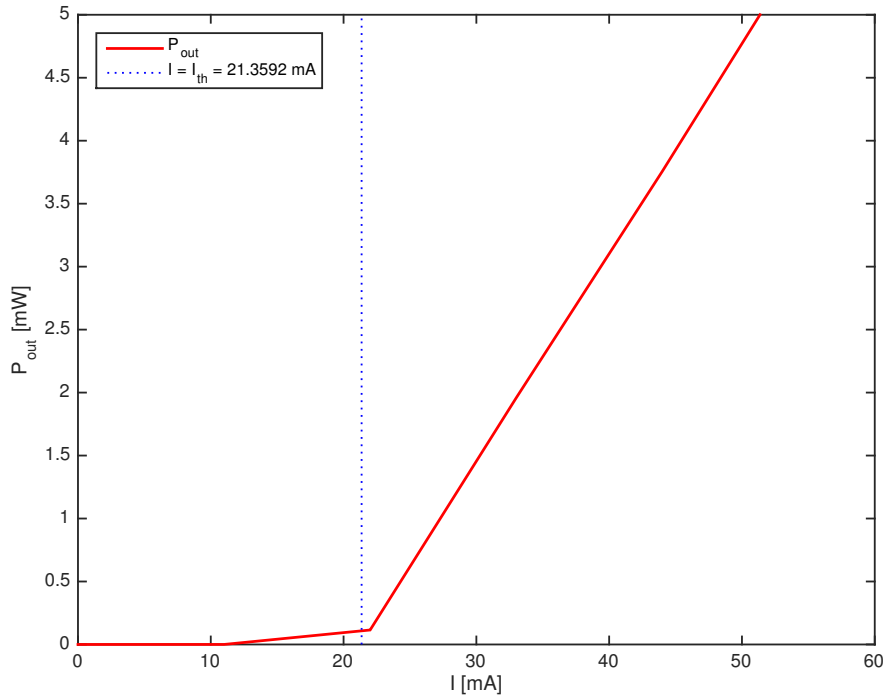
Figure 3.10: Light output (P_{out}) vs. current (I).

can see how small the photon density and thus the power is because the gain is not large enough to compensate the losses, hence what we see on the left part of the graph is mainly produced by spontaneous emission. Once the current increases and approaches the threshold I_{th}, the gain increases and the photon density starts to grow. Once exceeded the threshold, the gain equals the losses and the lasing

begins. That is what we see on the right part of the graph, where the photon density (and output power) increase linearly with the current, due to stimulated emission.

Note that for all the figures shown above, we used the most typical values in terms of dimensions and intrinsic properties of the cavity for conventional semiconductor lasers, and thus we adjusted and scaled the results in the graphs in order to represent the simulations. The main reason to do that is because there are few orders of magnitude between parameters, and so it is difficult to show the results properly scaled on the same graph. Nonetheless, it shows a good approximation to the theory and gives an idea of how semiconductor lasers work.

However, as we will discuss in the next section, the performance of a semiconductor laser worsens when we try to shrink its size and operating wavelength. Since one of our goals is to fulfill the requirements of nanotechnology, we carried out another simulation with the same kind of device, but this time we tried it out for a nanoscale configuration and for an operating frequency around 600 THz.

The results showed a bad performance of the laser in terms of both dynamic response and light-output curve. The main issue we observed was that the smaller the size of the cavity, the higher losses the laser experienced. This translates to the gain medium not able to compensate the absorption of photons from the cavity as well as the losses from the end mirrors. Therefore, stimulated emission processes were practically inexistent, thus no multiplication of photons was achieved.

That led us to think of other configurations, with different structures and materials. In the next section we summarize and discuss the suitability of a semiconductor laser for optical nanoscale communications and we propose a different alternative which represents a huge leap from conventional semiconductor lasers.

3.5 Outlook

Throughout this chapter we have seen the basic theory concerning semiconductor lasers, the equations that govern their dynamic response as well as the output characteristic when we apply a biased current. Last, we put all the theory presented together and simulated a basic semiconductor laser using MATLAB. Although recent implementations and novel techniques in the fabrication of semiconductor lasers allow these to work under room temperature and be as small as the operating wavelength, there are some aspects that makes us go beyond in the research of the most suitable signal source for our optical nanoscale communication system. The reason why we feel the need to go beyond semiconductor lasers is because after thorough study of these devices, their properties and performance in such conditions do not seem appropriate enough for what we are trying to achieve.

The first issue we encountered was that most of the semiconductor lasers work at infrared or near-infrared wavelengths ($1.55\ \mu m$), making them impossible to work at optical frequencies due to the high dissipation losses. Although recent techniques and implementations allow subwavelength cavity configurations, semiconductor lasers would be inefficient because they would hardly support plasmonic modes. An optical source that couples electronic transitions directly to strongly localized optical modes is highly desirable because it would avoid the limitations of delivering light from a macroscopic external source to a nanometer scale plasmonic waveguide, such as low coupling efficiency and difficulties in accessing individual optical modes. Recent studies, however, have come up with a new class of optical sources capable of exciting and amplifying surface plasmons. These are called plasmon lasers or SPASERs (**S**urface **P**lasmon **A**mplification by **S**timulated **E**mission of **R**adiation), and are the focus of our next chapter.

CHAPTER 4

Plasmon Nanolasers

In this chapter we propose a better and more suitable option for the demands of nanotechnology. As we mentioned in Section 3.5 and throughout this work, our goals were to shrink the size of the main components in a wireless communication system down to the nanometer scale, which that implicitly implied the change of perspective in the way material and electromagnetic waves behave; as well as to work at optical frequencies—which it also affects both the material and EM waves. That led us to surface plasmon-polaritons as the electromagnetic waves to carry the information throughout the communications system.

4.1   Introduction

Plasmon nanolasers constitute a new concept of optical source that have emerged in the recent years. They are nanoscale optical sources capable of exciting and amplifying SPP waves. Surface plasmon-polaritons show a great promise for an exciting new class of light sources capable of reconciling photonic and electronic

length scales [34]. Moreover, SPPs are capable of extremely strong mode confinement, enabling plasmon lasers to deliver intense, coherent and directional optical energy well below the diffraction limit.

The working principle of the first devices reported to date [33, 34] consist in creating an interface between a dielectric layer and metallic surface, where the electromagnetic waves (photons) hybridize with the surface plasmons existing in dielectric-metal interface. Then, by adding a high-quality semiconductor gain material, we are able to achieve surface plasmon-polariton radiation (Figure 4.1).

(a) CdS nanopatch from [33].

(b) CdS nanowire from [34].
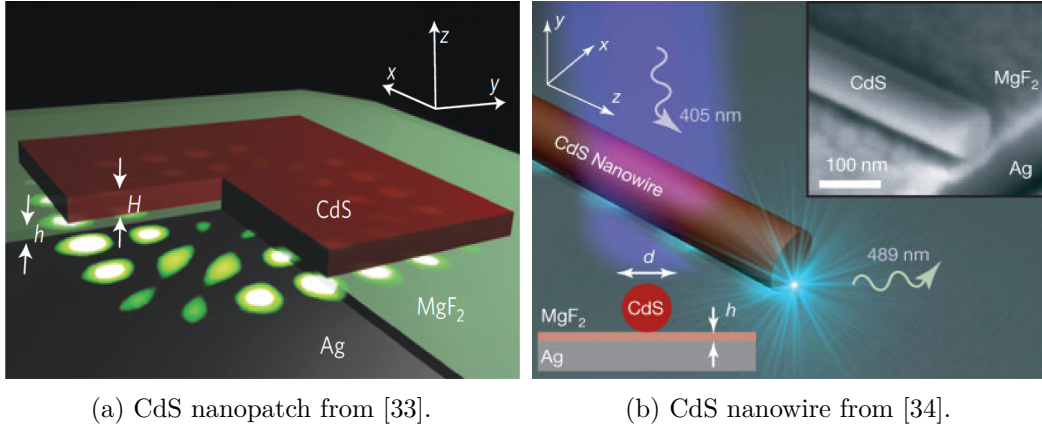
Figure 4.1: Different configurations for plasmon nanolasers. The CdS compound acts as the gain medium, while the interface between the thin dielectric layer of MgF_2 and the Ag substrate enable the excitation and propagation of SPP modes.

4.2 Basics

As the size of a laser is shrunk to the nanometer scale, both the gain medium and cavity have to be treated quantum mechanically. This constitutes a huge leap from conventional semiconductor lasers to the aforementioned nanolasers. The quantum properties of the optical mode of the nanocavity, such as the Purcell effect [37]

due to the strong confinement of the optical modes, become important. Moreover, the dispersion of the material, which is usually neglected in semiconductor lasers, is no longer negligible for plasmon nanolasers. For example, the confinement factor Γ traditionally used in Fabry-Pérot cavities for semiconductor lasers can be negative due to negative real part of the permittivity in metals. Indeed, the material inhomogeneity and dispersion are usually not critical when it comes to semiconductor lasers. However, for plasmonic nanolasers these are not true, since the metals exhibit negative and dispersive permittivities in these configurations. Therefore, all these differences have to be properly reflected on the equations that describe the operation of a laser, the rate equations. That is why we need a new formulation which takes into account the effects of the material dispersion and inhomogeneity from the very beginning.

In the next sections, we follow the methodology introduced in [8–10] to characterize plasmonic nanolasers. The notation is slightly different from the one we used in Chapter 3, since nanolasers are treated from a quantum point of view.

4.3 Fundamental Formulation

4.3.1 Optical Mode in Dispersive and Inhomogeneous Media

First, let us begin with a certain optical mode oscillating at frequency ω, its electric field can be expressed in the phasor form as

$$E(r,t) = \frac{\mathcal{E}(r)\mathrm{e}^{-i\omega t} + \mathcal{E}^*(r)\mathrm{e}^{i\omega t}}{2}, \tag{4.1}$$

where $\mathcal{E}(r)$ is the electric-field phasor of the optical mode. If we think of the phasor field $\mathcal{E}(r)$ as a single-photon field, its energy has to be quantified as

$$\hbar\omega = \int_V \frac{\varepsilon_0}{2} \frac{[\varepsilon'_g(r,\omega) + \varepsilon'_r(r,\omega)]}{2} |\mathcal{E}(r)|^2 \mathrm{d}r \tag{4.2}$$

where the quantity $\hbar\omega$ represents a single-photon energy. In (4.2),

$$\varepsilon'_g(r,\omega) = \left.\frac{\partial[\omega'\varepsilon'_r(r,\omega')]}{\partial\omega'}\right|_{\omega'=\omega} \tag{4.3}$$

is the real part of the relative group permittivity, $\varepsilon'_r(r,\omega)$ is the real part of the relative permittivity, and ε_0 is the vacuum permittivity. In (4.2), the term proportional to $\varepsilon'_g(r,\omega)$ comes from the electric energy in the dispersive medium whereas the term proportional to $\varepsilon'_r(r,\omega)$ denotes the magnetic energy. For plasmonic nanocavities, the introduction of the averaged permittivity $[\varepsilon'_g(r,\omega) + \varepsilon'_r(r,\omega)]/2$ ensures the integrand in (4.2) to be always positive [9].

One can also make use of the modal profile function $f(r)$, which is the analogous to the wave functions in Schrödinger's equation [7]:

$$\mathcal{E}(r) \equiv -i\sqrt{\frac{2\hbar\omega}{\varepsilon_0}} f(r), \tag{4.4}$$

$$1 = \int_V \frac{[\varepsilon'_g(r,\omega) + \varepsilon'_r(r,\omega)]}{2} |f(r)|^2 \mathrm{d}r. \tag{4.5}$$

4.3.2   Rate Equations for Nanolasers

Similarly to what we introduced in Section 3.2 for semiconductor lasers, the rate equations are powerful tools to understand the basics of semiconductor lasers and even using the simple forms of these equations, one can understand most of the

processes that take place in the cavity. For that reason, let us begin with a similar but different notation and form for the rate equations, this time in terms of the carrier number N_e in the active region and the total photon number S' of the lasing mode:

$$\frac{\partial N_e}{\partial t} = \eta_i \frac{I}{q} - R'_{nr} - R'_{sp} - R'_{st} S' \tag{4.6}$$

$$\frac{\partial S'}{\partial t} = R'_{st} S' - \frac{S'}{\tau_p} + \beta_{sp} R'_{sp} \tag{4.7}$$

where η_i is the injection efficiency, I the injection current $[A]$, q is the electron charge, R'_{nr} is the total nonradiative recombination rate $[s^{-1}]$, R'_{sp} is the total spontaneous emission rate $[s^{-1}]$, R'_{st} is the total stimulated emission rate $[s^{-1}]$, β_{sp} is the spontaneous emission factor, and τ_p is the photon lifetime $[s]$, expressed as follows from [10]:

$$\tau_p^{-1} = \tau_{p,mat}^{-1} + \tau_{p,rad}^{-1}, \tag{4.8}$$

where $\tau_{p,mat}$ and $\tau_{p,rad}$ are its components from material and radiation loss. One can also write the photon lifetime τ_p in terms of the lasing frequency ω and the quality factor of the lasing mode Q_t as:

$$\begin{aligned}
\frac{1}{Q_t} &= \frac{1}{Q} - \frac{R'_{st}}{\omega} \\
&= \frac{2\Delta\omega}{\omega} \\
&= \frac{1}{\tau_p\omega}.
\end{aligned} \tag{4.9}$$

Hence we obtain:

$$\tau_p^{-1} = \frac{\omega}{Q_t}, \tag{4.10}$$

with

$$\frac{1}{Q} = \frac{1}{Q_{mat}} + \frac{1}{Q_{rad}}, \tag{4.11}$$

where in (4.9), $\Delta\omega$ is the linewidth of the lasing mode. In (4.11), $Q_{mat} = \omega\tau_{p,mat}$ and $Q_{rad} = \omega\tau_{p,rad}$ are the quality factor contributions due to material and radiation loss of the lasing mode (excluding the contribution from laser medium). Q represents the quality factor when the gain medium is absent (transparent). Despite (4.6) and (4.7), the "famous" rate equations used by the scientific community (and as we stated in Chapter 3) are written by means of the carrier density N $[m^{-3}]$ and photon density S $[m^{-3}]$:

$$\frac{\partial N}{\partial t} = \eta_i \frac{I}{qV_a} - R_{nr}(N) - R_{sp}(N) - R_{st}(N)S \tag{4.12}$$

$$\frac{\partial S}{\partial t} = \Gamma R_{st}(N)S - \frac{S}{\tau_p} + \Gamma\beta_{sp}(N)R_{sp}(N) \tag{4.13}$$

with

$$N = \frac{N_e}{V_a}, \qquad\qquad S = \frac{S'}{V_{eff}}, \qquad\qquad \Gamma \equiv \frac{V_a}{V_{eff}}, \tag{4.14}$$

where V_a is the volume of the active region $[m^3]$, V_{eff} is the effective modal volume $[m^3]$, Γ is the confinement factor, and $R_{nr}(N), R_{sp}(N)$ and $R_{sp}(N)$ are obtained from their counterparts in (4.6) and (4.7) as follows:

$$R_{nr}(N) = \frac{R'_{nr}}{V_a} = \frac{N}{\tau_s} + CN^3 \tag{4.15}$$

$$R_{sp}(N) = \frac{R'_{sp}}{V_a} \tag{4.16}$$

$$R_{st}(N) = \frac{R'_{st}}{\Gamma} \tag{4.17}$$

where τ_s is the carrier recombination lifetime and C is the Auger recombination coefficient. The interesting thing about the confinement factor Γ is that it arises from the fact that the two densities N and S are defined on two different volumes V_a and V_{eff}, respectively (see eq. (4.14)). In most of the semiconductor lasers (Section 3.2.2.1), the volume of the active region V_a is well defined whereas the effective modal volume V_{eff} is usually not. The arbitrariness of V_{eff} originates from the nature of the electromagnetic wave which spreads out in real space and leads to the ambiguity of the confinement factor Γ. The use of $\Gamma = \Gamma_E$ as the energy confinement factor and the relation $V_{eff} = V_a/\Gamma_E$ leads to the natural definition of effective modal volume. One would have to define first the confinement factor Γ, and then calculate V_{eff} from (4.14). Also note that in (4.17), $R_{st}(N)$ depends on the confinement factor and thus depends on how the effective modal volume is defined. Traditionally, the stimulated emission rate $R_{st}(N)$ is written in terms of the material gain $g_m(N)$ of the active region and the group velocity v_g as the following:

$$R_{st}(N) = v_g g_m(N). \tag{4.18}$$

Since the quantity R'_{st} takes into account the effects of modal distribution and overlap with the active region, does not depend on how the effective modal volume is defined. Therefore, we obtain two different quantities which are independent of the effective modal volume V_{eff} as

$$\Gamma R_{st}(N) = R'_{st}, \tag{4.19}$$

$$\Gamma v_g = \frac{R'_{st}}{g_m(N)}. \tag{4.20}$$

Although $R_{st}(N)$, Γ and v_g depend on how one defines V_{eff}, their product do not. So the next step is to find the definitions for Γ and v_g which give a physical interpretation of the rate equations.

4.3.3 Spontaneous and Stimulated Emission Rates and Confinement Factor

In order to define the confinement factor Γ and thus the effective modal volume V_{eff} and stimulated emission rate $R_{st}(N)$, let us introduce a *slowly-varying* approximation of the spontaneous and stimulated emission rates derived from Fermi's Golden rule via the real-space approach from [8, 10] as:

$$R_{sp}(N) \simeq \sum_n \frac{1}{V_a} \left[\int_{V_a} \frac{|\mathcal{E}_n(r)|^2}{4} \mathrm{d}r \right] \frac{2\pi}{\hbar} \frac{\mu_{cv}^2}{V_a}$$
$$\times \sum_{c,v,K} \frac{\gamma_n}{\pi} \frac{p_{c,K}(1 - p_{v,K})}{(E_{c,K} - E_{v,K} - \hbar\omega_n)^2 + \gamma_n^2} \quad (4.21)$$

$$R_{st}(N) \simeq \frac{V_{eff}}{V_a} \left[\int_{V_a} \frac{|\mathcal{E}(r)|^2}{4} \mathrm{d}r \right] \frac{2\pi}{\hbar} \frac{\mu_{cv}^2}{V_a}$$
$$\times \sum_{c,v,K} \frac{\gamma}{\pi} \frac{p_{c,K} - p_{v,K}}{(E_{c,K} - E_{v,K} - \hbar\omega)^2 + \gamma^2} \quad (4.22)$$

where the indexes c, v correspond to the initial state in the conduction band c and final state in the valence band v. The variable $K = [k_c + k_v]/2$ is the averaged momentum of the conduction and valence wave vectors k_c and k_v, respectively[1]. γ is the linewidth of the optical transition, ω_n is the frequency of mode n, and $\gamma_n = \gamma + \hbar\omega_n/Q_n$ is the total linewidth including the broadening from the quality

---

[1] $|c, k_c\rangle$ and $|v, k_v\rangle$ represent the Bloch states near the Brillouin zone [12, p. 107-113].

factor Q_n. The terms $p_{c,K}$ and $p_{v,K}$ are the corresponding occupation probabilities of electrons in either conduction band c and valence band v, whereas $E_{c,K}$ and $E_{v,K}$ are the corresponding energies in those two bands. The term $\hbar\omega$ in (4.22) is the photon energy of the lasing mode. In (4.21), however, the summation over all optical modes (n) is necessary in order to obtain the spontaneous emission rate. Last, μ_{cv} represents the magnitude of the interband dipole moment [8, App. A]. From the density-matrix formalism [11], the imaginary part of the susceptibility contributed from the gain medium can be expressed as

$$\chi_a''(\omega) = -\frac{\pi}{\varepsilon_0} \frac{\mu_{cv}^2}{V_a} \sum_{c,v,K} \frac{\gamma}{\pi} \frac{p_{c,K} - p_{v,K}}{(E_{c,K} - E_{v,K} - \hbar\omega)^2 + \gamma^2}, \qquad (4.23)$$

therefore the stimulated emission rate $R_{st}(N)$ becomes

$$R_{st}(N) = -\frac{1}{2\hbar} \frac{V_{eff}}{V_a} \left[\int_{V_a} \varepsilon_0 |\mathcal{E}(r)|^2 \mathrm{d}r \right] \chi_a''(\omega). \qquad (4.24)$$

The imaginary part of the susceptibility $\chi_a''(\omega)$ is related to the material gain $g_m(\hbar\omega)$ of the active region as

$$g_m(\hbar\omega) = -\frac{\omega}{c} \frac{\chi_a''(\omega)}{n_a(\omega)} \qquad (4.25)$$

$$n_a(\omega) = \left[\frac{\varepsilon_{r,a}'(\omega) + \sqrt{\varepsilon_{r,a}'^2(\omega) + \varepsilon_{r,a}''^2(\omega)}}{2} \right]^{1/2} \qquad (4.26)$$

where $n_a(\omega)$ is the refractive index of the active region, which contains the contributions from the real and imaginary parts of the relative permittivity $\varepsilon_{r,a}'(\omega)$ and $\varepsilon_{r,a}''(\omega)$ in the active region, respectively. Using the expression in (4.25), we

can rewrite (4.24) in terms of the material gain $g_m(\hbar\omega)$ as

$$R_{st}(N) = \frac{V_{eff}}{V_a} \left[\frac{\int_{V_a} \varepsilon_0 |\mathcal{E}(r)|^2 \mathrm{d}r}{\hbar\omega} \right] \frac{n_a(\omega)c}{2} g_m(\hbar\omega). \tag{4.27}$$

Using the $\hbar\omega$-normalization defined in (4.2), (4.27) becomes

$$R_{st}(N) = \frac{V_{eff}}{V_a} \left[\frac{\int_{V_a} \frac{\varepsilon_0}{4}[\varepsilon'_{g,a}(\omega) + \varepsilon'_{r,a}(\omega)]|\mathcal{E}(r)|^2 \mathrm{d}r}{\int_{V} \frac{\varepsilon_0}{4}[\varepsilon'_{g}(r,\omega) + \varepsilon'_{r}(r,\omega)]|\mathcal{E}(r)|^2 \mathrm{d}r} \right]$$
$$\times \left[\frac{2n_a(\omega)}{\varepsilon'_{g,a}(\omega) + \varepsilon'_{r,a}(\omega)} \right] c g_m(\hbar\omega), \quad (4.28)$$

where $\varepsilon'_{g,a}(\omega)$, $\varepsilon'_{r,a}(\omega)$ are the real parts of the group permittivity and relative permittivity in the active region, respectively. The first term in brackets of (4.28) is defined as the energy confinement factor $\Gamma = \Gamma_E$ as follows:

$$\Gamma_E \equiv \frac{\int_{V_a} \frac{\varepsilon_0}{4}[\varepsilon'_{g,a}(\omega) + \varepsilon'_{r,a}(\omega)]|\mathcal{E}(r)|^2 \mathrm{d}r}{\int_{V} \frac{\varepsilon_0}{4}[\varepsilon'_{g}(r,\omega) + \varepsilon'_{r}(r,\omega)]|\mathcal{E}(r)|^2 \mathrm{d}r}. \tag{4.29}$$

The second term in brackets of (4.28) can be simplified to the inverse of the material group index $n_{g,a}(\omega)$ if we assume the term of the imaginary part $\varepsilon''_{r,a}(\omega)$ in (4.26) is irrelevant:

$$\frac{\varepsilon'_{g,a}(\omega) + \varepsilon'_{r,a}(\omega)}{2n_a(\omega)} \approx \frac{1}{2n_a(\omega)} \left[\left. \frac{\partial[\omega' n_a^2(\omega')]}{\partial\omega'} \right|_{\omega'=\omega} + n_a^2(\omega) \right]$$
$$= \left. \omega' \frac{\partial n_a(\omega')}{\partial\omega'} \right|_{\omega'=\omega} + n_a(\omega) \tag{4.30}$$
$$= \left. \frac{\partial[\omega' n_a(\omega')]}{\partial\omega'} \right|_{\omega'=\omega} + n_{g,a}(\omega).$$

Now, from (4.29) and (4.30), the stimulated emission rate $R_{st}(N)$ can be written in its simple form when we define the effective modal volume as

$$V_{eff} = \frac{V_a}{\Gamma_E}, \tag{4.31}$$

$$R_{st}(N) = \upsilon_{g,a}(\omega) g_m(\hbar\omega), \tag{4.32}$$

where $\upsilon_{g,a}(\omega) = c/n_{g,a}(\omega)$ is the material group velocity of the active region. It is important to notice that in (4.29), the energy confinement factor $\Gamma_E < 1$, which makes physical sense, since an optical mode cannot totally overlap with the gain medium. This condition still holds onto a plasmonic cavity, where the real part of the metal permittivity is negative [9].

With the results obtained for the confinement factor $\Gamma = \Gamma_E$ and therefore the effective modal volume V_{eff} and stimulated emission rate $R_{st}(N)$, the rate equations for a plasmonic nanolaser (4.12) and (4.13) are now well defined.

4.3.4 Characterization to a Fabry-Pérot Cavity

Fabry-Pérot cavities are the most common waveguides used for both semiconductor lasers and plasmonic nanolasers. In order to follow a similar procedure like in Chapter 3 (Section 3.2.1), we will apply the concepts that we have presented in previous sections of this chapter to Fabry-Pérot cavities.

For a Fabry-Pérot cavity length L, the expression for the amplitude of the lasing mode can be approximated to the one of a standing wave (superposition of two counterpropagating waves) for $z \in (0, L)$ as the following:

$$\mathcal{E}(r) \simeq \mathcal{E}(\rho)F(z)e^{ik_z z} + \tilde{\mathcal{E}}(\rho)B(z)e^{-ik_z z}, \tag{4.33}$$

where k_z is the corresponding propagation constant of the mode, $F(z)$ and $B(z)$ are the forward and backward amplitudes of the counterpropagating waves that satisfy the boundary conditions at the two ends of the cavity. $\mathcal{E}(\rho)$ is the transverse profile of the waveguide mode (transverse coordinates ρ), and $\mathcal{E}(\rho)$ and $\tilde{\mathcal{E}}(\rho)$ have identical transverse components but opposite longitudinal components $(\tilde{\mathcal{E}}_z(\rho) = -\mathcal{E}_z(\rho))$. If we take the normalization condition from (4.2), for the Fabry-Pérot case is

$$\hbar\omega = \int_0^L \mathrm{d}z \int_A \mathrm{d}\rho \frac{\varepsilon_0}{4} \left\{ [|F(z)|^2 + |B(z)|^2]|\mathcal{E}(\rho)|^2 \right.$$
$$+ 2\,\mathrm{Re}[\mathcal{E}(\rho)\tilde{\mathcal{E}}^*(\rho)F(z)B^*(z)e^{2ik_zz}] \Big\}$$
$$\times [\varepsilon_g'(\rho,\omega) + \varepsilon_r'(\rho,\omega)] + \int \text{outside of the cavity.} \quad (4.34)$$

where A is the total cross section of the cavity. The last term in (4.34) is a contribution form the residual field outside the cavity region. From (4.34), one can factorize the normalization condition as follows:

$$\int_A \mathrm{d}\rho \frac{\varepsilon_0}{4} [\varepsilon_g'(\rho,\omega) + \varepsilon_r'(\rho,\omega)]|\mathcal{E}(\rho)|^2 = \hbar\omega \qquad (4.35)$$

$$\int_0^L \mathrm{d}z[|F(z)|^2 + |B(z)|^2]$$
$$+ \text{effective} \int \text{outside of the cavity} = 1 \qquad (4.36)$$

where $\varepsilon_g'(\rho,\omega)$ and $\varepsilon_r'(\rho,\omega)$ now depend on the transverse coordinates ρ, assuming that the gain and losses do not affect much on the translational invariance of $\varepsilon_g'(\rho,\omega)$ and $\varepsilon_r'(\rho,\omega)$ along the cavity direction, and the integration of the oscillatory part in (4.34) is neglected. The approximation of the integral from outside the cavity in (4.34) for an effective value in (4.36) leads to the introduction of an effective

longitudinal confinement factor Γ_z as

$$\Gamma_z \equiv \int_0^L [|F(z)|^2 + |B(z)|^2]\mathrm{d}z, \tag{4.37}$$

which is close to one in most Fabry-Pérot-based cavities, whose active region and cavity are the same in length.

4.3.4.1 Energy Confinement Factor $(\Gamma = \Gamma_E)$

Now, if we assume a uniform material gain along the z-direction, the stimulated emission rate $R_{st}(N)$ from (4.27) can be expressed as

$$R_{st}(N) = \frac{V_{eff}}{V_a}\Gamma_z \left[\frac{\int_{A_a} \varepsilon_0 |\mathcal{E}(\rho)|^2 \mathrm{d}\rho}{\hbar\omega}\right] \frac{n_a(\omega)c}{2} g_m(\hbar\omega), \tag{4.38}$$

where A_a is the cross section of the active region. Following the same procedure like in Section 4.3.3, we obtain a new confinement factor $\Gamma = \Gamma_E$, defined by the longitudinal confinement factor Γ_z and a certain transverse energy confinement factor $\Gamma_{E,t}$ as:

$$\Gamma_E = \Gamma_z \Gamma_{E,t}, \tag{4.39}$$

$$\Gamma_{E,t} = \frac{\int_{A_a} \frac{\varepsilon_0}{4}[\varepsilon'_{g,a}(\omega) + \varepsilon'_{r,a}(\omega)]|\mathcal{E}(\rho)|^2 \mathrm{d}\rho}{\int_A \frac{\varepsilon_0}{4}[\varepsilon'_g(\rho,\omega) + \varepsilon'_r(\rho,\omega)]|\mathcal{E}(\rho)|^2 \mathrm{d}\rho}, \tag{4.40}$$

which in turn gives a new definition for the effective modal volume V_{eff} for a Fabry-Pérot cavity as

$$V_{eff} = \frac{V_a}{\Gamma_E} = \frac{V_a}{\Gamma_z \Gamma_{E,t}}. \tag{4.41}$$

With the results obtained for the confinement factor $\Gamma = \Gamma_E$ and therefore the effective modal volume V_{eff} and stimulated emission rate $R_{st}(N)$, the rate

equations for a plasmonic nanolaser (4.12) and (4.13) are now well defined for a Fabry-Pérot cavity.

4.3.4.2 Waveguide Confinement Factor $(\Gamma = \Gamma_M)$

Now, if we solve the photon density rate equation (4.13) in steady state $(\frac{\partial S}{\partial t} = 0)$, we can obtain the threshold condition for the nanolaser as follows:

$$0 = \Gamma R_{st}(N)S - \frac{S}{\tau_p} + \Gamma \beta_{sp}(N)R_{sp}(N). \tag{4.42}$$

Ignoring the spontaneous emission term in (4.42) and using the expression in (4.18) we obtain:

$$0 = \Gamma R_{st}(N_{th}) - \frac{1}{\tau_p} \tag{4.43}$$

$$0 = \Gamma v_g g_{th}(\hbar\omega) - \frac{1}{\tau_p} \tag{4.44}$$

where N_{th} is the threshold carrier density and $g_{th}(\hbar\omega)$ is the threshold material gain of the active region. As we stated for Fabry-Pérot cavities in Chapter 3 (Section 3.2.2.3), the threshold gain must satisfy the condition for one complete roundtrip oscillation:

$$0 = \Gamma_z \tilde{g}_{th}(\hbar\omega) - \alpha_s - \frac{1}{2L} \ln\left(\frac{1}{R_1 R_2}\right), \tag{4.45}$$

where we used $\tilde{g}(\hbar\omega) = \Gamma g_m(\hbar\omega)$ as the modal gain. The term α_s represents the intrinsic modal losses of the waveguide, and the last term represents the losses due to the end facets of the cavity (R_1, R_2). Comparing (4.44) with (4.45), we can write the confinement factor Γ as the product $\Gamma_z \Gamma_t$, where Γ_t is a certain

transverse confinement factor which satisfies

$$\tilde{g}(\hbar\omega) = \Gamma_t g_m(\hbar\omega). \tag{4.46}$$

Then, we can define the photon lifetime τ_p as

$$\frac{1}{\tau_p} = \upsilon_{g,z}\left[\alpha_s + \frac{1}{2L}\ln\left(\frac{1}{R_1 R_2}\right)\right], \tag{4.47}$$

where $\upsilon_{g,z}$ is the waveguide group velocity along the z-direction.

Since $\Gamma \upsilon_g = \Gamma_z \Gamma_t \upsilon_g$ does not depend on V_{eff} (see (4.20)), and Γ_t has been defined by the modal gain in (4.46), the group velocity $\upsilon_{g,z}$ is not arbitrary anymore, otherwise the photon lifetime τ_p would depend on V_{eff}, which makes no physical sense.

Now, taking back the modal gain $\tilde{g}(\hbar\omega)$, we can express it in terms of the Poynting theorem from [28, 41] as:

$$\tilde{g}(\hbar\omega) = \frac{c n_a(\omega) \int_{A_a} \frac{\varepsilon_0}{2}|\mathcal{E}(\rho)|^2 \mathrm{d}\rho}{P_z} g_m(\hbar\omega), \tag{4.48}$$

where P_z is the propagating power flow along the z-direction, which is the surface of the real part of the Poynting vector $S(\rho)$ as

$$P_z = \int_a \mathrm{Re}[S(\rho)]\mathrm{d}\rho \cdot \hat{z}, \tag{4.49}$$

$$S(\rho) = \frac{1}{2}[\mathcal{E}(\rho) \times \mathcal{H}^*(\rho)] \tag{4.50}$$

where $\mathcal{H}(\rho)$ is the transverse profile of the magnetic field $\mathcal{H}(r)$ as

$$\mathcal{H}(r) = \mathcal{H}(\rho)F'(z)e^{ik_z z} + \tilde{\mathcal{H}}(\rho)B'(z)e^{-ik_z z} \tag{4.51}$$

53

where $F'(z)$ and $B'(z)$ are the forward and backward amplitudes of the coun-terpropagating waves and $\mathcal{H}(\rho)$, $\tilde{\mathcal{H}}(\rho)$ have identical longitudinal components but opposite transverse components $(\tilde{\mathcal{H}}_\perp(\rho) = -\mathcal{H}_\perp(\rho))$. If we compare (4.46) and (4.48) we obtain the transverse confinement factor Γ_t as

$$\begin{aligned}\Gamma_t \equiv \Gamma_{wg} &= \frac{cn_a(\omega)\int_{A_a}\frac{\varepsilon_0}{2}|\mathcal{E}(\rho)|^2\mathrm{d}\rho}{P_z}\\ &= \frac{n_a(\omega)}{2\eta_0}\frac{\int_{A_a}|\mathcal{E}(\rho)|^2\mathrm{d}\rho}{P_z}\end{aligned} \tag{4.52}$$

where Γ_{wg} is the waveguide confinement factor and η_0 is the intrinsic impedance[2]. If we were to assume that the optical modes are weakly guided with a frequency much above the cutoff such that $|\mathcal{E}_z(\rho)| \ll |\mathcal{E}_t(\rho)|$ and $k_z/k_0 \simeq n_a(\omega)$, where $k_0 = \omega/c$ is the propagation constant, the waveguide confinement factor Γ_{wg} would approach the power confinement factor Γ_p, which is typically used by the semiconductor laser community:

$$\Gamma_p = \frac{\int_{A_a}\mathrm{Re}\left\{\frac{1}{2}[\mathcal{E}(\rho)\times\mathcal{H}^*(\rho)]\right\}\mathrm{d}\rho\cdot\hat{z}}{\int_{A}\mathrm{Re}\left\{\frac{1}{2}[\mathcal{E}(\rho)\times\mathcal{H}^*(\rho)]\right\}\mathrm{d}\rho\cdot\hat{z}}. \tag{4.53}$$

For a strongly guided mode (or plasmonic mode), the confinement factor $\Gamma_t \equiv \Gamma_{wg}$ defined in (4.52) may exceed one. Thus the interpretation of Γ_{wg} as a confinement factor is mathematically correct but it lacks physical sense. Furthermore, the propagating power flow pointing at $\hat{z}$ in (4.53) may become negative for a plasma medium, which may lead to the wrong results. We will further discuss this approach in Section 4.5.

Now, in order to find an expression to characterize the waveguide group velocity

---

[2]Intrinsic impedance $\eta_0 = (\varepsilon_0 c)^{-1}$, where ε_0 and c are the permittivity and speed of light in vacuum, respectively.

introduced in (4.47), by taking the expression from (4.18) we obtain:

$$v_{g,z} = \frac{R_{st}(N)}{g_m(\hbar\omega)}.$$ (4.54)

Using the expressions for $R_{st}(N)$ in (4.38), and the confinement factor Γ as:

$$\Gamma = \frac{V_a}{V_{eff}}, \qquad\qquad \Gamma = \Gamma_z\Gamma_t, \qquad\qquad \Gamma_t = \Gamma_{wg}, \qquad (4.55)$$

we obtain

$$v_{g,z} = \frac{P_z}{\hbar\omega} = \frac{\int_A \mathrm{Re}\left\{\frac{1}{2}[\mathcal{E}(\rho) \times \mathcal{H}^*(\rho)]\right\}\mathrm{d}\rho \cdot \hat{z}}{\int_A \frac{\varepsilon_0}{4}[\varepsilon_g'(\rho,\omega) + \varepsilon_r'(\rho,\omega)]|\mathcal{E}(\rho)|^2\mathrm{d}\rho}.$$ (4.56)

It can be proved from [8] that under a lossless and nonmagnetic condition, the waveguide group velocity in (4.56) along the z-direction can be written as

$$\frac{1}{v_{g,z}(\omega)} = \frac{\int_A \frac{\varepsilon_0}{4}[\varepsilon_g'(\rho,\omega) + \varepsilon_r'(\rho,\omega)]|\mathcal{E}(\rho)|^2\mathrm{d}\rho}{\int_A \mathrm{Re}\left\{\frac{1}{2}[\mathcal{E}(\rho) \times \mathcal{H}^*(\rho)]\right\}\mathrm{d}\rho \cdot \hat{z}}$$

$$= \frac{\partial k_z(\omega)}{\partial\omega}.$$ (4.57)

Hence, we obtain another set of rate equations based on total waveguide confinement factor $\Gamma = \Gamma_M$ given by

$$\Gamma_M = \Gamma_z\Gamma_{wg},$$ (4.58)

$$\Gamma_{wg} = \frac{n_a(\omega)}{2\eta_0}\frac{\int_{A_a}|\mathcal{E}(\rho)|^2\mathrm{d}\rho}{\int_A \mathrm{Re}\left\{\frac{1}{2}[\mathcal{E}(\rho) \times \mathcal{H}^*(\rho)]\right\}\mathrm{d}\rho \cdot \hat{z}},$$ (4.59)

which defines a new effective modal volume in terms of the waveguide confinement factor Γ_M as

$$V_{eff} = \frac{V_a}{\Gamma_M} = \frac{V_a}{\Gamma_z\Gamma_{wg}}.$$ (4.60)

Now we can write the expression for the photon lifetime τ_p in terms of the waveguide group velocity $\upsilon_{g,z}(\omega)$, which no longer depends on the confinement factor used:

$$\frac{1}{\tau_p} = \upsilon_{g,z}(\omega) \left[\alpha_s + \frac{1}{2L} \ln \left(\frac{1}{R_1 R_2} \right) \right].\qquad(4.61)$$

In this section we have presented a model for plasmonic nanolasers. By taking into account the singularities of materials in such configurations and inspecting the concept of confinement factor in different situations, we have formulated the equations that describe plasmonic nanolasers. We have seen that the energy confinement factor Γ_E and material group velocity $\upsilon_{g,a}(\omega)$ of the active region are well defined and give a good interpretation for both general configuration of nanolasers and Fabry-Pérot cavities, while the concept of waveguide confinement factor Γ_{wg} and waveguide group velocity $\upsilon_{g,z}(\omega)$ in Fabry-Pérot cavities might not always be a good choice, since Γ_{wg} may exceed one when $\upsilon_{g,z}(\omega)$ is too low, which leads to the wrong results.

4.4 Plasmon Nanolaser Simulation with COMSOL *Multi-physics*

Similarly to what we did in Section 3.4 for semiconductor lasers, we carried out a simulation of a plasmon nanolaser, this time using the multi-physics software COMSOL running on our supercomputing cluster facility (*the UB Center for Computational Research*).

We opted to reproduce a similar structure to what *Ma et al.* did in [26], which consists of a 45-nm-thick cadmium sulphide (CdS) nanopatch atop a silver surface separated by a 5-nm-thick magnesium fluoride (MgF$_2$) gap layer (see Figure 4.2). The close proximity between the high-permittivity CdS nanopatch and the silver surface enables modes of the CdS to hybridize with the surface plasmons of the dielectric-metal interface, leading to strong confinement of light in the gap region with relatively low metal loss.
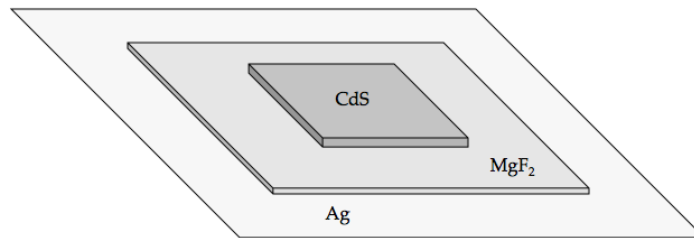
Figure 4.2: Plasmon nanolaser layout.

4.4.1 Definition of the Nanolaser Structure

The first step is to define a set of global parameters to determine the geometry of the nanolaser. The global parameters for the nanolaser can be found in Appendix C.2,

and the resulting built structure is shown in Figure 4.3. To guarantee the accuracy of the simulation and to minimize the number of reflections from the simulation space boundaries, we define a *Perfectly Matched Layer* or PML, which is the sphere-like structure surrounding the whole nanopatch shown in Figure 4.3e.

(a)   (b)   (c)

(d)   (e)
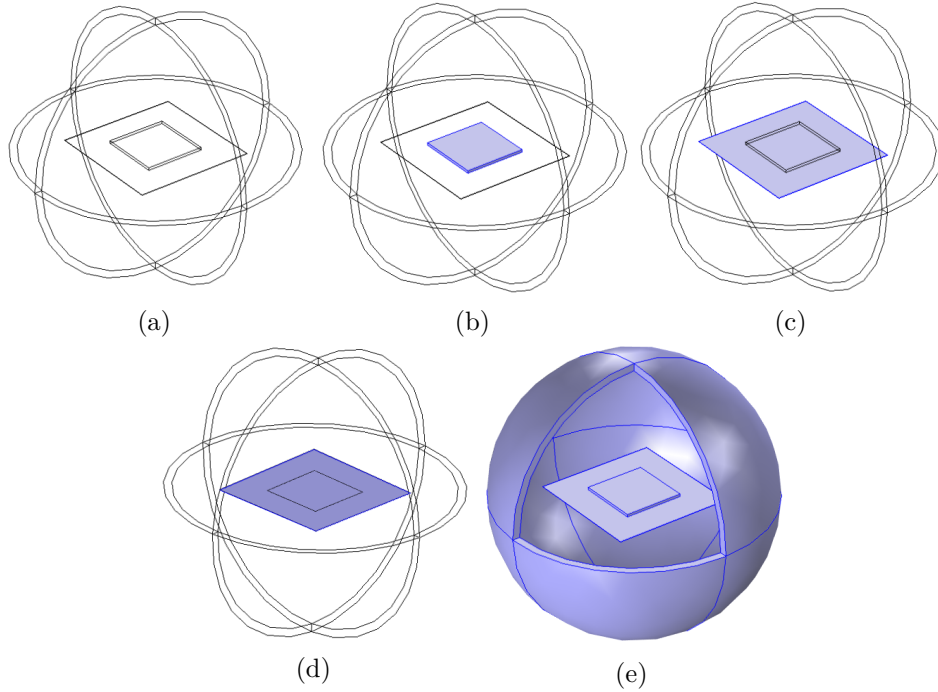
Figure 4.3: Plasmon nanolaser layout with COMSOL. The purple-colored zones in (b), (c) and (d) represent the CdS layer, the MgF_2 layer and the Ag surface, respectively. (e) shows the sliced-sphere PML surrounding the entire nanostructure.

The next step consists in assigning the corresponding material to each layer. For that, the gain medium is defined by the relative permittivity of CdS, which can be modeled as the following expression from [26]:

$$\varepsilon_{CdS} = 4.23 + \frac{\lambda^2}{\lambda^2 - 0.18},$$
(4.62)

58

where λ is the operating wavelength. Then, the gap layer of MgF_2 is defined by its refractive index $n_{MgF_2} = 1.374$. As for the metallic surface, since it will act as the ground plane, in COMSOL we define it as a boundary condition, which is the bottom face of the dielectric layer (Figure 4.3d). If we wanted to be realistic with the simulations, we should define the metallic surface by its optical properties for this particular case, given by the expression of complex permittivity for metals at high frequencies extracted from the *Drude-Lorentz* model (see Appendix C.1). However, as a first approach and to save computation time, we will consider the ground plane as a Perfect Electric Conductor (PEC), which we define in the next part.

4.4.2   Frequency Domain Study

In order to analyze the response of the laser, we define a new *Electromagnetic Waves, Frequency Domain* study in COMSOL. We use the frequency form of the wave equation to be solved by the simulator. Then, since the ground plane is modeled as a PEC, we assign the corresponding boundary as a new Perfect Electric Conductor condition in COMSOL.

The next thing we need for the simulation is a source of excitation. For that matter, we define a plane wave as:

$$E_z = E_0 e^{-ik_0 y}, \tag{4.63}$$

where E_0 is the amplitude and k_0 the propagation constant at the frequency under study. The electromagnetic wave propagates along y-direction and "illuminates" the structure, exciting the gain medium within the laser.

The last step before running the simulation is to define the mesh structure. The mesh creates a "web" of certain number of elements in which the solver computes the equations. The recommended maximum element size for the mesh to guarantee accuracy in the results is $\lambda/5$, where λ refers to the wavelength at the frequency under study. Since our structure contains very small sections (*i.e.*, the 5-nm thick gap layer), a much finer mesh needs to be defined separately. The resulting meshed geometry is shown in Figure 4.4. An extremely fine mesh is defined on the MgF_2 layer (blue-colored layer), a less finer mesh is defined for the CdS nanopatch and finally for the PML we define a swept mesh.
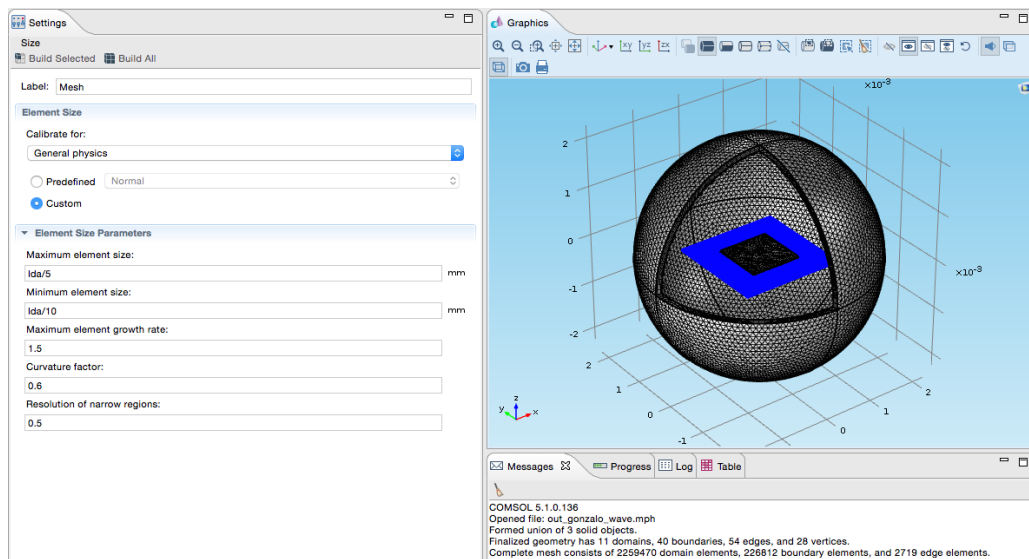
Figure 4.4: Meshed geometry. The mesh element size is defined by "lda", which is the wavelength at the frequency under study. For the blue-colored zone and the dark top patch we defined a much finer mesh to capture all the fine features.

4.4.3   Simulation Results

Once the structure is properly defined, it is time to call the solver. In this case, we carried out a frequency domain simulation for one single operating frequency of 600 THz. The simulation results are shown in Figure 4.5. The electric field distribution within the cavity clearly shows a confined TM-like mode[3] that has not completely hybridized with the surface plasmons existing at the dielectric-metal interface. The expected SPP modes should be reflected at the cavity boundaries, but since this is a non-resonant mode, we only see weak field confinement at those boundaries (all 4 corners in the nanopatch).

In order to obtain resonant modes in the cavity we should compute an eigenfrequency study, in which the solver tries to find resonant frequencies around a center frequency fixed by the user.

Figure 4.5: Plasmon nanolaser simulation with COMSOL. (a) and (b) show the electric field distribution confined in the interface between the MgF_2 layer and the Ag surface.

---

[3]TM $\equiv$ Transverse Magnetic mode.

Unfortunately, we are unable to show an eigenfrequency study in this work, mainly due to the complexity in the geometry and computation capacity and time required to solve this system in particular. To give the re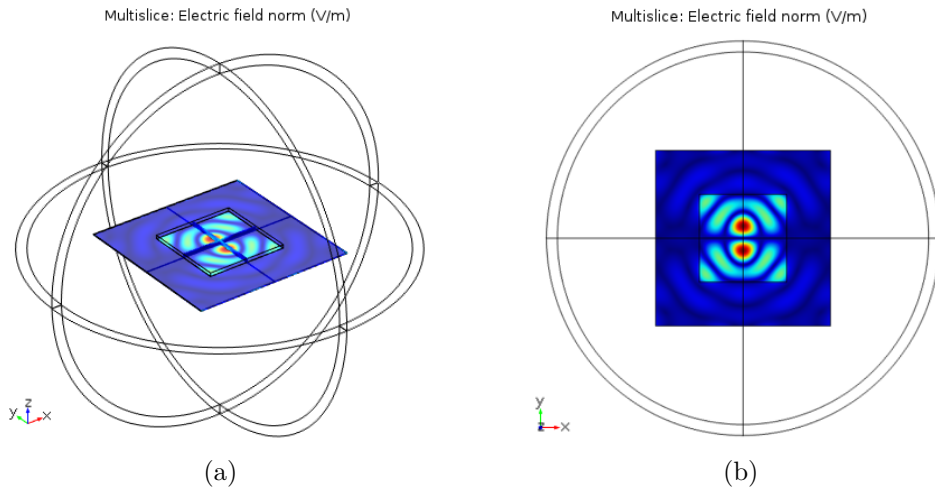ader an idea of how much computation is needed, the results shown in Figure 4.5 were carried out in one of our supercomputer nodes. This specific node consists in 16 cores working at 2.20 GHz with 128 GB of RAM, in which the simulation for just one computed frequency took up to 8 hours. The complexity in the geometry, the fine sections like the 5-nm-thick gap layer in front of the 1-μm-long nanopatch require an extremely fine mesh to capture all the features without losing accuracy. Although we tried different approaches to obtain the corresponding eigenfrequencies in one of our High Memory Compute nodes (32 cores with 256 GB of RAM), we were unable to obtain any good results due to a timeout/memory failure in the cluster. That led us to consider other alternatives for future simulations: i) redefine the mesh structure increasing the maximum element size; ii) split the simulation into a 2D+1D approach; iii) adjust the parameters in COMSOL for cluster computing.

4.5   Outlook

In this chapter we have presented the fundamental formulation for plasmonic nanolasers. By taking into account the effects on the metals at optical frequencies as well as the cavity phenomena at the nanometer scale, we introduced a new set of rate equations that describe the operation of such devices. The fact that plasmonic nanolasers need to be treated quantum mechanically requires a change in our mindset, since light-matter interactions in such small configurations differ from what we had seen to date.

Then, we carried out a simulation of a plasmon nanolaser with COMSOL in our

supercomputing cluster facility. We described all the steps to define the structure, select the frequency study and finally run the simulation. The results obtained were not optimal, since we were unable to fully represent the plasmonic modes confined at the cavity boundaries. The main reason was that we encountered some major issues in terms of the complexity in the geometry vs. the computation time needed to solve the equations. For that matter, we proposed different alternatives to solve this problem for future simulations.

Although plasmon lasers show a great promise for an exciting new class of light sources, they still are at very early stages. Recent studies have demonstrated the realization of such nanolasers, enabling the excitation and amplification of SPP waves under optical pumping at room temperature. Despite that, all plasmon lasers reported to date have not been able to operate under electrical injection/pumping. The main reason is that electrical injection introduces high dissipation losses, making the plasmon lasers unable to operate at room temperature. That means we require a light source (semiconductor laser) to provide with sufficient energy feedback in order to make a plasmon nanolaser work, which it makes the whole system bulky and inefficient, unable to satisfy the requirements of nanotechnology. The realization of a plasmon nanolaser capable of working under electrical injection constitutes the main challenge for the future.

CHAPTER 5

Conclusions and Future Work

In this thesis, we presented the basics of wireless optical communications in the nanoscale, in which we described the state-of-the-art devices to date that deal with the manipulation of surface plasmon-polaritons, strongly localized electromagnetic waves existing at a dielectric-metal interface. The exceptional properties of these modes make them suitable to propagate in nanometer scale regions, being able to carry our information through the communication system. For that purpose, as the main focus of this work two different alternatives of light sources to achieve surface plasmon-polariton excitation and amplification were proposed.

First, we revised the fundamentals of semiconductor lasers, which are the most common light sources in optical communications. We described their working principles and validate them in a simulation with MATLAB. Although recent implementations and advanced techniques demonstrated the ability for semiconductor lasers to work under some of the conditions imposed by nanotechnology, they still are not suitable for optical nanoscale communications. We identified the

challenges when going into the nanometer scale for semiconductor lasers and we came up with an exciting, new class of light source: plasmonic nanolasers.

We presented the fundamental formulation for plasmonic nanolasers, taking into account the effects on the material and the cavity in such nanoscale configurations and at optical frequencies. Last, we presented a plasmon nanolaser simulation with the multi-physics software COMSOL in our supercomputing facility. After the first results came out, we realised how important the geometry in nanoscale lasers is. Even though we ran the simulations in our supercomputer, we were unable to obtain good enough results to fully characterize plasmonic nanolasers.

Our future research directions include the further and thorough study of plasmonic nanolasers through better understanding of the quantum theory behind the formulation and through large scale simulations. Eventual development of experimental prototypes are considered as well for the future. However, to the best of our knowledge, a plasmon nanolaser working under electrical injection at room temperature has not been demonstrated yet. Besides the arduous fabrication process of nanoscale plasmon lasers, a major challenge is posed by the limitations in the laser feeding source, since electrical injection introduces high dissipation losses, making nanolasers unable to work at room temperature. Along with this challenge, achieving stimulated amplification of surface plasmon-polaritons at visible frequencies constitutes another great challenge owing to the intrinsic ohmic losses of metals.

Optical nanoscale communications is a very new research area within the broad field of communications and networks. The realization and integration of nanoscale components into a nanomachine to communicate among nanonetworks will enable a whole new range of long-awaited applications in many fields of our society.

L-I Formulation

In Sections 3.3.1 and 3.3.2:

$$N = \frac{\eta_i \tau_s}{qV_a} I \tag{A.1}$$

$$S = \frac{\beta_{sp} \eta_i I}{\left(\frac{1}{\tau_p} - A\left(\frac{\eta_i \tau_s}{qV_a} I - N_0\right)\right) qV_a}, \tag{A.2}$$

where in (A.2),

$$A = \Gamma a \upsilon_g,$$

and

$$g_m = a(N - N_0) = a\left(\frac{\eta_i \tau_s}{qV_a} I - N_0\right).$$

Appendix A. L-I Formulation

In Sections 3.3.2 to 3.3.4, the threshold carrier density N_{th} is the carrier density at which the gain reaches the threshold—that is, the gain equals the losses and the lasing begins. Using the expressions found in (3.3), (3.17) and (3.18):

$$\tilde{g}(N_{th}) = \Gamma g_m(N_{th}) = \alpha_t \tag{A.3}$$

$$\alpha_t = \alpha_s + \alpha_m \tag{A.4}$$

$$g_m(N_{th}) = a(N_{th} - N_0) \tag{A.5}$$

$$\tilde{g}(N_{th}) = \Gamma a(N_{th} - N_0) \tag{A.6}$$

we obtain the following equation

$$\Gamma a(N_{th} - N_0) = \alpha_t. \tag{A.7}$$

Therefore, the expression for the carrier density at threshold is:

$$N_{th} = N_0 + \frac{\alpha_t}{\Gamma a}. \tag{A.8}$$

MATLAB Simulation

B.1   InGaAs Semiconductor Laser Parameters

Table B.1

Cavity parameters		
Parameter	Quantity	Value
d	Height	0.2 μm
L	Length	500 μm
w	Width	2 μm
λ	Operating wavelength	1.55 μm

Table B.2

Physical constants		
Parameter	Quantity	Value
c	Speed of light in vacuum	$3 \times 10^8\ ms^{-1}$
h	Planck's constant	$6.626 \times 10^{-34}\ m^2 kgs^{-1}$
q	Electron charge	$1.602 \times 10^{-19}\ C$

Table B.3

Intrinsic parameters		
Parameter	Quantity	Value
τ_s	Carrier lifetime	$3\ ns$
τ_p	Photon lifetime	$1\ ps$
Γ	Confinement factor	0.17
n	Refractive index	3.4
R_1	Reflective index	0.3
R_2	Reflective index	0.3
a	Gain coefficient	$6.67 \times 10^{-20}\ m^2$
N_0	Transparency carrier density	$10^{24}\ m^{-3}$
β_{sp}	Spontaneous emission factor	10^{-4}

Table B.4

Derived parameters			
Parameter	Quantity	Expression	Value
f	Operating frequency	$\frac{c}{\lambda}$	$193.55\ THz$
υ_g	Group velocity	$\frac{c}{n}$	$8.82 \times 10^7\ ms^{-1}$
A_a	Area of active region	$d \times w$	$0.4\ \mu m^2$
V_a	Volume of active region	$A_a \times L$	$200\ \mu m^3$
α_t	Total losses	$\frac{1}{\tau_p \upsilon_g}$	$1.13 \times 10^4\ m^{-1}$
α_m	Mirror losses	$\frac{1}{2L} \ln\left(\frac{1}{R_1 R_2}\right)$	$0.24 \times 10^4\ m^{-1}$
η_o	Output coupling efficiency	$\frac{\alpha_m}{\alpha_t}$	0.22

B.2   MATLAB Script

```matlab
%%%%%%%%%%%%%%%%%%%%%%%%%%%%%%%%%%%%%%%%%%%%%%%%%%%%%%%%%%%%%%%%%%%%%%%%%%%%
%%%%%%%%%%%%%%%%%%%%%%%%%%%%%%%% SCRIPT %%%%%%%%%%%%%%%%%%%%%%%%%%%%%%%%%%%%
%%%%%%%%%%%%%%%%%%%%%%%%%%%%%%%%%%%%%%%%%%%%%%%%%%%%%%%%%%%%%%%%%%%%%%%%%%%%
clear all
close all
clc
%%%%%%%%%%%%%%%%%%%%%%% CONSTANTS AND PARAMETERS %%%%%%%%%%%%%%%%%%%%%%%%%%%
tau_s = 3e-9; % Carrier lifetime
tau_p = 1e-12; % Photon lifetime
gamma = 0.17; % Confinement factor
q = 1.602e-19; % Electron charge
c = 3e8; % Speed of Light in vaccum
vg = c/3.4; % Group velocity
a = 1e-12/(gamma*vg); % gain coefficient
A = gamma*a*vg; % gain factor
N0 = 1e24; % Transparency carrier density
S0 = 1/(A*tau_s); % Term to normalize S
beta = 1e-4; % Spontaneous emission factor
h = 6.625e-34; % Planck's constant
lambda = 1.55e-6; % Operating wavelength
f = c/lambda; % Operating frequency
d = 0.2e-6; % height
w = 2e-6; % width
area = d*w; % Area of active region
L = 500e-6; % length
V = area*L; % Volume of active region
I0 = N0*q*V/tau_s; % Transparency current
I = 0; %Initial value for bias current
```

70

```matlab
tau_n = tau_s/tau_p; % Normalized tau
eta = A*tau_p*N0; % Term to normalize rate equations
R = 0.3; % Reflective index (R1 = R2)
effi = 1; %injection efficiency
alpha_t = 1/(vg*tau_p); % Total losses (a_s+a_m)
alpha_m = (1/(2*L))*log(1/R^2); % Mirror losses
effo = alpha_m/alpha_t; %output coupling efficiency
%%%%%%%%%%%%%%%%%%%%%%%%%%%%%%%%%%%%%%%%%%%%%%%%%%%%%%%%%%%%%%%%%%%%%%%%%%

%%%%%%%%%%%%%%%%%%%%%%%%%%%% RATE EQUATIONS %%%%%%%%%%%%%%%%%%%%%%%%%%%%%%
TSPAN = [0 10]; % Time span for the differential equations
Y0 = [0 0]; % Initial conditions for both N and S
[T,Y] = ode45(@rate_equations,TSPAN,Y0,[],I); % Calling to the equations solver
% Representation of the carrier density 'N' along time 't'
H = figure(1);
set(H,'color','w');
subplot(2,1,1)
plot(tau_s*1e9*T, Y(:,1), 'r', 'Linewidth', 1)
%title('Carrier density in the upper lasing level')
xlabel('time [ns]')
ylabel('N ( x 10^{24} [m^{-3}] )')
% Locate threshold carrier density
Nth = Y(end,1); % Threshold Carrier density
hold all
% Plot Nth constant in the same graph
line(TSPAN,[Nth Nth], 'Color', 'k', 'LineStyle', ':')
% Find the switch-on delay of the laser
idx = find(Y>Nth,1,'first'); % Find the first time N ~ Nth
td = T(idx)*tau_s*1e9; % Switch-on delay (fix units in ns)
% Represent the switch-on delay within the carrier density graph
line([td td], ylim, 'Color', 'b', 'LineStyle', ':')
```

71

```matlab
legend('N', 'N = N_{th}', 't = t_{d}', 'Location', 'SouthEast')
axis auto
% Representation of the photon density 'S' along time 't'
subplot(2,1,2)
plot(tau_s*1e9*T,Y(:,2)*S0*1e-20, 'b', 'Linewidth', 1)
%title('Photon density in active region')
ylabel('S ( x 10^{20} [m^{-3}] )')
xlabel('time [ns]')
axis auto
% Locate Son parameter, which is the photon density level at which lasing
% occurs
Son = Y(end,2)*S0*1e-20; % Lasing mode (fix units)
line(xlim,[Son Son], 'Color', 'k', 'LineStyle', ':')
legend('S', 'S = S_{on}', 'Location', 'NorthEast')
H = figure(2);
set(H,'color','w');
Po = effo*V*h*f*S0.*Y(:,2)./tau_p; % Output power
plot(tau_s*1e9*T,Po*1e3, 'k')
%title('Output Power')
ylabel('P_{out} [mW]')
xlabel('time [ns]')
%%%%%%%%%%%%%%%%%%%%%%%%%%%%%%%%%%%%%%%%%%%%%%%%%%%%%%%%%%%%%%%%%%%%%%%%%%%%%

%%%%%%%%%%%%%%%%%%%%%%%%%% L-I CHARACTERISTIC %%%%%%%%%%%%%%%%%%%%%%%%%%%%%%%%
% Calculate the threshold current, the limit at which the laser is working
% under stimulated emission instead of spontaneous emission
Ith = q*V*Nth/tau_s; % Threshold current
Ith = Ith*N0; % fix magnitude
Ith = Ith*1e3; % fix units

N = 10; % Number of samples (the more samples, the more resolution)
```

```matlab
% Create empty arrays for both S and current
S = zeros(1,N);
current = zeros(1,N);
I = 0; % Initial condition for the pumping current
d_I = 11e-3; % Rate at which the current increases
% Loop in which we will call to the equations solver for each iteration
% and we will store the current values for both photon density 'S'
% and current 'I'
for i=1:N
    [T,Y] = ode15s(@rate_equations2,TSPAN,Y0,[],I);
    S(i) = Y((length(Y(:,2))),2);
    current(i) = I;
    I = I + d_I;
end
% Once we have all the values stored in the arrays, we will calculate the
% output power, which depends on the photon density 'S'
Pout = effo*V*h*f*S*S0/tau_p; % Output power
% We create a new window to represent the L-I characteristic
H = figure(3);
set(H,'color','w');
% Representation of the Light-output vs current of the laser
plot(current*1e3,Pout*1e3, 'r','LineWidth', 1.5)
hold all
%title('L - I characteristic')
xlabel('I [mA]')
ylabel('P_{out} [mW]')
axis([0 60 0 5])
line([Ith Ith], ylim, 'Color', 'b', 'LineStyle', ':')
legend('P_{out}', ['I = I_{th} = ',num2str(Ith), ' mA'], 'Location', 'NorthWest')
%%%%%%%%%%%%%%%%%%%%%%%%%%%%%%%%%%%%%%%%%%%%%%%%%%%%%%%%%%%%%%%%%%%%%%%%%%%%
%%%%%%%%%%%%%%%%%%%%%%%%%%%%%%%%%%%%%%%%%%%%%%%%%%%%%%%%%%%%%%%%%%%%%%%%%%%%
```

73

```matlab
%%%%%%%%%%%%%%%%%%%%%%%%%%%%%%%%%%%%%%%%%%%%%%%%%%%%%%%%%%%%%%%%%%%%%%%%%%%
%%%%%%%%%%%%%%%%%%%%%%%%% RATE EQUATIONS %%%%%%%%%%%%%%%%%%%%%%%%%%%%%%%%%%%
function dy = rate_equations(t,y,I)
% Create an array for both derivatives 'N' and 'S'
dy = zeros(2,1);
% Constants and parameters
tau_s = 3e-9; % Carrier lifetime
tau_p = 1e-12; % Photon lifetime
gamma = 0.17; % Confinement factor
c = 3e8; % Speed of Light in vaccum
vg = c/3.4; % Group velocity
a = 1e-12/(gamma*vg); % gain coefficient
A = gamma*a*vg; % gain factor
N0 = 1e24; % Transparency carrier density
beta = 1e-4; % Spontaneous emission factor
q = 1.602e-19; % Electron charge
d = 0.2e-6; % height
w = 2e-6; % width
area = d*w; % Area of active region
L = 500e-6; % length
V = area*L; % Volume of active region
effi = 1; % injection efficiency
I0 = N0*q*V/tau_s; % Transparency current
tau_n = tau_s/tau_p; % Norm tau
eta = A*tau_p*N0; % Norm term for the equations
% For the first case (rate equations) we will use a constant pumping
% current fixed to a given value
I = 3*I0; % Injection current
n = y(1); % Normalized carrier density (N/N0)
s = y(2); % Normalized photon density (S/S0)
k = tau_n*eta; % Term to simplify the equations
```

74

```matlab
% RATE EQUATIONS
dy(1)= effi*I/I0 - (n-1)*s - n; % dn/dT
dy(2) = k*(n-1)*s - tau_n*s + beta*k*n; % ds/dT
end
%%%%%%%%%%%%%%%%%%%%%%%%%%%%%%%%%%%%%%%%%%%%%%%%%%%%%%%%%%%%%%%%%%%%%%%%%%%%%
%%%%%%%%%%%%%%%%%%%%%%%%%%%%%%%%%%%%%%%%%%%%%%%%%%%%%%%%%%%%%%%%%%%%%%%%%%%%%
```

```matlab
%%%%%%%%%%%%%%%%%%%%%%%%%%%%%%%%%%%%%%%%%%%%%%%%%%%%%%%%%%%%%%%%%%%%%%
%%%%%%%%%%%%%%%%%%%%%%%%% L-I CHARACTERISTIC %%%%%%%%%%%%%%%%%%%%%%%%%%%%
% Note that in this case, 'I' is one of the arguments for the equations
function dy = rate_equations2(t,y,I)
% Create an array for both derivatives 'N' and 'S'
dy = zeros(2,1);
% Constants and parameters
tau_s = 3e-9; % Carrier lifetime
tau_p = 1e-12; % Photon lifetime
gamma = 0.17; % Confinement factor
c = 3e8; % Speed of Light in vaccum
vg = c/3.4; % Group velocity
a = 1e-12/(gamma*vg); % gain coefficient
A = gamma*a*vg; % gain factor
N0 = 1e24; % Transparency carrier density
beta = 1e-4; % Spontaneous emission factor
q = 1.602e-19; % Electron charge
d = 0.2e-6; % height
w = 2e-6; % width
area = d*w; % Area of active region
L = 500e-6; % length
V = area*L; % Volume of active region
effi = 1; % injection efficiency
I0 = N0*q*V/tau_s; % Transparency current
tau_n = tau_s/tau_p; % Norm tau
eta = A*tau_p*N0; % Norm term for the equations
n = y(1); % Normalized carrier density (N/N0)
s = y(2); % Normalized photon density (S/S0)
k = tau_n*eta; % Term to simplify the equations
```

```matlab
% RATE EQUATIONS

dy(1)= effi*I/I0 - (n-1)*s - n; % dn/dT

dy(2) = k*(n-1)*s - tau_n*s + beta*k*n; % ds/dT

end

%%%%%%%%%%%%%%%%%%%%%%%%%%%%%%%%%%%%%%%%%%%%%%%%%%%%%%%%%%%%%%%%%%%%%%%%%%%%%%%

%%%%%%%%%%%%%%%%%%%%%%%%%%%%%%%%%%%%%%%%%%%%%%%%%%%%%%%%%%%%%%%%%%%%%%%%%%%%%%%
```

COMSOL Simulation of a Plasmon Nanolaser

C.1 Drude-Lorentz Model for Noble Metals

The *Drude-Lorentz* model for noble metals at high frequencies, which accounts for the photons with higher energies, gives a good approximation for both interband and intraband transitions. The frequency-dependent relative permittivity $\varepsilon_r(\omega)$ is derived from solving the equation of motion for electrons excited by a time-harmonic electric field. Then, the relative complex permittivity is related to the conductivity $\sigma(\omega)$ as follows:

$$\sigma(\omega) = \sigma'(\omega) + i\sigma''(\omega) = \varepsilon_0 \omega \varepsilon_r(\omega), \tag{C.1}$$

$$\varepsilon_r(\omega) = \varepsilon_r'(\omega) + i\varepsilon_r''(\omega), \tag{C.2}$$

$$\varepsilon_r'(\omega) = 1 - \frac{\omega_p \tau_D^2}{1 + \omega^2 \tau_D^2}, \tag{C.3}$$

$$\varepsilon_r''(\omega) = \frac{\omega_p^2 \tau_D}{\omega(1 + \omega^2 \tau_D^2)}, \tag{C.4}$$

where $\omega_p = \sqrt{\frac{Ne^2}{m\varepsilon_0}}$ is the plasma frequency, N is the carrier density, e is the electron charge, m is the electron effective mass, ε_0 is the vacuum permittivity, ω is the operating frequency and τ_D is the electron relaxation time. Table C.1 shows the optical constant values for different noble metals [21, 42].

Table C.1

Metal	$\omega_p(\times 10^{15}\ rad/s)$	$\tau_D(\times 10^{-14}\ s)$	$N(\times 10^{28}\ m^{-3})$
Al	22.8	26	18.1
Au	13.8	3.3	5.9
Ag	**13.4**	**0.8**	**5.9**
Cu	14.1	0.8	8.5

Optical parameters for different noble metals

C.2   Plasmon Nanolaser Parameters

▼ **Parameters**

Name	Expression	Value	Description
D	5[nm]	5E-9 m	MgF2 layer thickness
W_patch	1000[nm]	1E-6 m	CdS patch width
L_patch	1000[nm]	1E-6 m	CdS patch length
E0	1[V/m]	1 V/m	Incident field amplitude
f0	600[THz]	6E14 Hz	Operating freqeuncy
lda	c_const/f0	4.9965E-7 m	Wavelength
k0	2*pi*f0/c_const	1.2575E7 1/m	Propagation constant
r0	max(2*L_patch,2*W_patch)	2E-6 m	Radius
nd	1.374	1.374	MgF2 refractive index
W_subs	2*W_patch	2E-6 m	MgF2 layer width
L_subs	2*L_patch	2E-6 m	MgF2 layer length
R0	r0+lda/2	2.2498E-6 m	PML radius

Figure C.1: Plasmon nanolaser parameters.

Bibliography

[1] Ian F Akyildiz and Josep Miquel Jornet. Electromagnetic wireless nanosensor networks. *Nano Communication Networks*, 1(1):3–19, 2010.

[2] Ian F Akyildiz and Josep Miquel Jornet. The internet of nano-things. *IEEE Wireless Communications*, 17(6):58, 2010.

[3] David J Bergman and Mark I Stockman. Surface plasmon amplification by stimulated emission of radiation: quantum generation of coherent surface plasmons in nanosystems. *Physical review letters*, 90(2):027402, 2003.

[4] Pierre Berini and Israel De Leon. Surface plasmon-polariton amplifiers and lasers. *Nature Photonics*, 6(1):16–24, 2012.

[5] Max Born and Emil Wolf. *Principles of optics: electromagnetic theory of propagation, interference and diffraction of light.* Cambridge university press, 1999.

[6] Sergey I Bozhevolnyi, Valentyn S Volkov, Eloise Devaux, Jean-Yves Laluet, and Thomas W Ebbesen. Channel plasmon subwavelength waveguide components including interferometers and ring resonators. *Nature*, 440(7083):508–511, 2006.

[7] Siegmund Brandt and Hans Dieter Dahmen. *The picture book of quantum mechanics.* Springer Science & Business Media, 2012.

[8] Shu-Wei Chang and Shun Lien Chuang. Fundamental formulation for plasmonic nanolasers. *Quantum Electronics, IEEE Journal of*, 45(8):1014–1023, 2009.

[9] Shu-Wei Chang and Shun Lien Chuang. Normal modes for plasmonic nanolasers with dispersive and inhomogeneous media. *Optics letters*, 34(1):91–93, 2009.

[10] Shu-Wei Chang, Chi-Yu Adrian Ni, and Shun-Lien Chuang. Theory for bowtie plasmonic nanolasers. *Optics express*, 16(14):10580–10595, 2008.

[11] Shun Lien Chuang and Shun L Chuang. *Physics of optoelectronic devices*. Wiley New York, 1995.

[12] Supriyo Datta. *Quantum transport: atom to transistor*. Cambridge University Press, 2005.

[13] K Ding and CZ Ning. Metallic subwavelength-cavity semiconductor nanolasers. *Light: Science & Applications*, 1(7):e20, 2012.

[14] Kang Ding, MT Hill, ZC Liu, LJ Yin, PJ van Veldhoven, and CZ Ning. Record performance of electrical injection sub-wavelength metallic-cavity semiconductor lasers at room temperature. *Optics express*, 21(4):4728–4733, 2013.

[15] Kang Ding, ZC Liu, LJ Yin, MT Hill, MJH Marell, PJ Van Veldhoven, R Nöetzel, and CZ Ning. Room-temperature continuous wave lasing in deep-subwavelength metallic cavities under electrical injection. *Physical Review B*, 85(4):041301, 2012.

[16] H Ditlbacher, FR Aussenegg, JR Krenn, B Lamprecht, G Jakopic, and G Leising. Organic diodes as monolithically integrated surface plasmon polariton detectors. *Applied physics letters*, 89(16):161101–161101, 2006.

[17] Jens Dorfmuller, Ralf Vogelgesang, Worawut Khunsin, Carsten Rockstuhl, Christoph Etrich, and Klaus Kern. Plasmonic nanowire antennas: experiment, simulation, and theory. *Nano letters*, 10(9):3596–3603, 2010.

[18] Abram L Falk, Frank HL Koppens, L Yu Chun, Kibum Kang, Nathalie de Leon Snapp, Alexey V Akimov, Moon-Ho Jo, Mikhail D Lukin, and Hongkun Park. Near-field electrical detection of optical plasmons and single-plasmon sources. *Nature Physics*, 5(7):475–479, 2009.

[19] Dmitry Yu Fedyanin, Alexey V Krasavin, Aleksey V Arsenin, and Anatoly V Zayats. Surface plasmon polariton amplification upon electrical injection in highly integrated plasmonic circuits. *Nano letters*, 12(5):2459–2463, 2012.

[20] Dmitri K Gramotnev and Sergey I Bozhevolnyi. Plasmonics beyond the diffraction limit. *Nature Photonics*, 4(2):83–91, 2010.

[21] Peter B Johnson and R-W_ Christy. Optical constants of the noble metals. *Physical Review B*, 6(12):4370, 1972.

[22] Josep Miquel Jornet and Ian F Akyildiz. Fundamentals of electromagnetic nanonetworks in the terahertz band. *Foundations and Trends® in Networking*, 7(2-3):77–233, 2013.

[23] M Khajavikhan, A Simic, M Katz, JH Lee, B Slutsky, A Mizrahi, V Lomakin, and Y Fainman. Thresholdless nanoscale coaxial lasers. *Nature*, 482(7384):204–207, 2012.

[24] James C Lin. *Electromagnetic fields in biological systems*. CRC press, 2011.

[25] Ansheng Liu, Richard Jones, Ling Liao, Dean Samara-Rubio, Doron Rubin, Oded Cohen, Remus Nicolaescu, and Mario Paniccia. A high-speed silicon optical modulator based on a metal–oxide–semiconductor capacitor. *Nature*, 427(6975):615–618, 2004.

[26] Ren-Min Ma, Rupert F Oulton, Volker J Sorger, Guy Bartal, and Xiang Zhang. Room-temperature sub-diffraction-limited plasmon laser by total internal reflection. *Nature materials*, 10(2):110–113, 2011.

[27] Stefan Alexander Maier. *Plasmonics: fundamentals and applications: fundamentals and applications*. Springer Science & Business Media, 2007.

[28] AV Maslov and CZ Ning. Modal gain in a semiconductor nanowire laser with anisotropic bandstructure. *Quantum Electronics, IEEE Journal of*, 40(10):1389–1397, 2004.

[29] A Melikyan, L Alloatti, A Muslija, D Hillerkuss, PC Schindler, J Li, R Palmer, D Korn, S Muehlbrandt, Dries Van Thourhout, et al. High-speed plasmonic phase modulators. *Nature Photonics*, 8(3):229–233, 2014.

[30] Pieter Neutens, Pol Van Dorpe, Iwijn De Vlaminck, Liesbet Lagae, and Gustaaf Borghs. Electrical detection of confined gap plasmons in metal–insulator–metal waveguides. *Nature Photonics*, 3(5):283–286, 2009.

[31] Maziar P Nezhad, Aleksandar Simic, Olesya Bondarenko, Boris Slutsky, Amit Mizrahi, Liang Feng, Vitaliy Lomakin, and Yeshaiahu Fainman. Room-temperature subwavelength metallo-dielectric lasers. *Nature Photonics*, 4(6):395–399, 2010.

[32] Thomas Nikolajsen, Kristjan Leosson, and Sergey I Bozhevolnyi. Surface plasmon polariton based modulators and switches operating at telecom wavelengths. *Applied Physics Letters*, 85(24):5833–5835, 2004.

[33] MA Noginov, G Zhu, AM Belgrave, Reuben Bakker, VM Shalaev, EE Narimanov, S Stout, E Herz, T Suteewong, and U Wiesner. Demonstration of a spaser-based nanolaser. *Nature*, 460(7259):1110–1112, 2009.

[34] Rupert F Oulton, Volker J Sorger, Thomas Zentgraf, Ren-Min Ma, Christopher Gladden, Lun Dai, Guy Bartal, and Xiang Zhang. Plasmon lasers at deep subwavelength scale. *Nature*, 461(7264):629–632, 2009.

[35] Edward D Palik. *Handbook of optical constants of solids*, volume 3. Academic press, 1998.

[36] David FP Pile and Dmitri K Gramotnev. Nanoscale fabry–pérot interferometer using channel plasmon-polaritons in triangular metallic grooves. *Applied Physics Letters*, 86(16):161101, 2005.

[37] Edward M Purcell. Spontaneous emission probabilities at radio frequencies. *Physical Review*, 69:681, 1946.

[38] Graham T Reed, G Mashanovich, FY Gardes, and DJ Thomson. Silicon optical modulators. *Nature photonics*, 4(8):518–526, 2010.

[39] John M Senior. *Optical fiber communications: principles and practice*, volume 2. Prentice Hall UK, 1992.

[40] Mark I Stockman. The spaser as a nanoscale quantum generator and ultrafast amplifier. *Journal of Optics*, 12(2):024004, 2010.

[41] TD Visser, H Blok, Bart Demeulenaere, and D Lenstra. Confinement factors and gain in optical amplifiers. *Quantum Electronics, IEEE Journal of*, 33(10):1763–1766, 1997.

[42] Paul R West, Satoshi Ishii, Gururaj V Naik, Naresh K Emani, Vladimir M Shalaev, and Alexandra Boltasseva. Searching for better plasmonic materials. *Laser & Photonics Reviews*, 4(6):795–808, 2010.

[43] Qianfan Xu, Bradley Schmidt, Sameer Pradhan, and Michal Lipson. Micrometre-scale silicon electro-optic modulator. *Nature*, 435(7040):325–327, 2005.